Published in final edited form as:

Circulation. 2021 September 07; 144(10): 805–822. doi:10.1161/CIRCULATIONAHA.120.053047.

Defective flow-migration coupling causes arteriovenous malformations in hereditary hemorrhagic telangiectasia

Hyojin Park, PhD[1], **Jessica Furtado, BS**[1], **Mathilde Poulet, PhD**[1], **Minhwan Chung, PhD**[1], **Sanguk Yun, PhD**[1], **Sungwoon Lee, PhD**[2], **William C Sessa, PhD**[2], **Claudio A Franco, PhD**[3,4], **Martin A Schwartz, PhD**[1,5], **Anne Eichmann, PhD**[1,6,7,*]

[1]Cardiovascular Research Center, Department of Internal Medicine, Yale University School of Medicine, New Haven CT, USA

[2]Yale University School of Medicine, Department of Pharmacology, New Haven CT, USA

[3]Instituto de Medicina Molecular João Lobo Antunes, Faculdade de Medicina, Universidade de Lisboa, Lisboa, Portugal

[4]Instituto de Histologia e Biologia do Desenvolvimento, Faculdade de Medicina, Universidade de Lisboa, Lisboa, Portugal

[5]Yale University School of Medicine, Departments of Cell Biology and Biomedical Engineering, New Haven CT, USA

[6]Yale University School of Medicine, Department of Molecular and Cellular Physiology, New Haven, CT, USA

[7]Université de Paris, PARCC, INSERM, F-75006 Paris, France

Abstract

Background: Activin receptor-like kinase 1 (ALK1) is an endothelial transmembrane serine threonine kinase receptor for BMP family ligands that plays a critical role in cardiovascular development and pathology. Loss-of-function mutations in the *ALK1* gene cause type 2 hereditary hemorrhagic telangiectasia (HHT), a devastating disorder that leads to arteriovenous malformations (AVMs). Here we show that ALK1 controls endothelial cell polarization against the direction of blood flow and flow-induced endothelial migration from veins through capillaries into arterioles.

Methods: Using Cre lines that recombine in different subsets of arterial, capillary-venous or endothelial tip cells, we showed that capillary-venous *Alk1* deletion was sufficient to induce AVM formation in the postnatal retina.

Results: ALK1 deletion impaired capillary-venous endothelial cell polarization against the direction of blood flow *in vivo* and *in vitro*. Mechanistically, ALK1 deficient cells exhibited increased integrin signaling interaction with VEGFR2, which enhanced downstream YAP/TAZ

[*]**Address for Correspondence:** Anne Eichmann, PhD, 333 Cedar St, SHM BE-36E, New Haven, CT, USA 06510, Tel: 203-218-8459, anne.eichmann@yale.edu.

Disclosures

None.

nuclear translocation. Pharmacological inhibition of integrin or YAP/TAZ signaling rescued flow migration coupling and prevented vascular malformations in *Alk1* deficient mice.

Conclusions: Our study reveals ALK1 as an essential driver of flow-induced endothelial cell migration and identifies loss of flow-migration coupling as a driver of AVM formation in HHT disease. Integrin-YAP/TAZ signaling blockers are new potential targets to prevent vascular malformations in HHT patients.

Keywords

HHT; arteriovenous malformations; mechanotransduction; Integrin; Hippo; BMP; VEGF

Introduction

Hereditary hemorrhagic telangiectasia (HHT) is an inherited autosomal dominant vascular disorder that causes arteriovenous malformations (AVMs) in more than 1.4 million people worldwide[1]. More than 90% of HHT cases are caused by heterozygous mutations in the endothelial surface receptors *ENG* (endoglin, mutated in HHT1) and *ALK1* (*ACVRL1*, mutated in HHT2), and mutations in *SMAD4* cause a combined juvenile polyposis-HHT syndrome that accounts for <5% of HHT cases[2–5]. ALK1 and ENG are receptors for TGF-β superfamily members BMP9 and BMP10[6, 7]. Ligand binding activates ALK1/ENG receptor signaling to cytoplasmic SMAD1/5/8, which subsequently complex with SMAD4 and translocate into the nucleus to regulate gene expression[8]. Thus, known HHT mutations affect different components of an endothelial signaling pathway that prevents vessels from forming AVMs. A recent study has shown that somatic second-hits inactivating the remaining intact *ALK1* or *ENG* allele occurred in the lesions, supporting that vascular malformations in HHT are caused by a two-hit mechanism[9].

Whereas the genetics of AVM have been well studied, the underlying cellular and molecular principles are not fully understood, thus limiting the development of new treatment options. AVMs are direct connections between arteries and veins that lack an intermediate capillary bed[2]. AVMs in HHT patients appear most often in the skin, oral cavity, nasal, and gastrointestinal (GI) tract mucosa, lung, liver, and brain. Small AVMs in the skin and mucus membranes are called telangiectasias; rupture of these lesions leads to frequent epistaxis, GI bleeding, and anemia, all of which are major quality of life issues for HHT patients[10]. Larger AVMs in liver, lung, or brain may additionally cause life-threatening conditions such as high output heart failure and stroke[11]. We and others previously showed that pan-endothelial knockout of *Alk1* using *Alk1*$^{f/f}$ *Cdh5 Cre*^{ERT2} in neonates led to AVMs in retina, brain and internal organs, indicating that endothelial ALK1 is necessary for proper vascular development[12, 13]. However, what types of ECs are responsible and how AVMs develop remain largely unknown.

Previous data from us and others have shown that BMP9/10-ALK1-ENG-SMAD4 signaling is enhanced by flow, and initiates a negative feedback signal that dampens flow-induced activation of AKT, thereby coordinating proper vascular remodeling[12, 14–17]. Mechanistically, blocking BMP9-ALK1-ENG signaling promotes endothelial phosphoinositide 3-kinase (PI3K)/AKT activation. ALK1 deficient ECs showed

enhanced phosphorylation of the PI3K target AKT and vascular endothelial growth factor receptor 2 (VEGFR2)[13, 18]. Pharmacological VEGFR2 or PI3K inhibition prevented AVM formation in *Alk1* deficient mice and decreased diameter of AVMs in *Eng* mutants[19]. Moreover, an increase in PI3K signaling has been recently confirmed in cutaneous telangiectasia biopsies of patients with HHT2[20, 21].

Here we investigated the origin of AVM-causing cells using novel Cre lines that delete *Alk1* in subsets of ECs. In doing so, we observed that ECs in remodeling vessels move against the direction of blood flow, while maintaining vascular integrity. In response to the physical forces such as wall shear stress exerted by blood, ECs polarize their Golgi apparatus in front of the nucleus (front-rear polarity) and migrate against the blood flow from veins towards arteries. We further provide evidence that ALK1 contributes to flow-migration coupling via VEGFR2-integrin signaling and downstream YAP/TAZ nuclear translocation. Collectively, the data show that ALK1 controls flow-induced cell migration to prevent AVM formation and identify new targets with the potential to prevent vascular malformations in HHT patients.

Methods

The data and methods supporting this study's findings are available from the corresponding author on request. Detailed methods are available in the Supplemental materials.

Mice

All animal experiments were performed under a protocol approved by Institutional Animal Care Use Committee of Yale University. The supplemental material contains a list of all mouse strains and protocols.

Statistical Analysis

All data are shown as mean ± standard error of the mean (SEM) and were analyzed using Student's t-test, one-way ANOVA with Sidak's multiple comparison test, and two-way ANOVA with Tukey's multiple comparison test or Sidak's multiple comparison test. All the statistical analyses were done using Prism 6 (GraphPad Software Inc., USA). ns: nonsignificant, $p>0.05$, * $p < 0.05$, ** $p < 0.01$, *** $p < 0.001$.

Results

Endothelial lineage tracing reveals flow-migration coupling in retinal vessels

To track the dynamics of endothelial flow-migration coupling in the mouse retina, we used three Cre^{ERT2} lines that recombine in subsets of ECs. These include Major Facilitator Superfamily Domain Containing 2a (MFSD2A), which recombines venous and capillary ECs but not arteries or tip cells in the brain vasculature[22–24]; Endothelial Cell-Specific Molecule 1 (ESM1), which recombines tip cells and their progeny[25, 26]; and the artery-specific BMX non-receptor tyrosine kinase (BMX)[27] lines. We intercrossed these lines with *mTmG* reporter mice[28] to lineage-trace GFP positive *Mfsd2a*, *Esm1* and *Bmx* expressing ECs. Tamoxifen (Tx) was injected 12 h, 24 h and 48 h prior to sacrifice at P6 (Figure

1A–1I). At 12 h post injection, *Mfsd2a*-positive cells were absent from the tip cell position, but labeled veins and capillaries in the vascular plexus, as well as the distal pole of arterioles (Figure 1A). *Esm1*-positive cells were restricted to the tip position, while *Bmx Cre^{ERT2}* positive cells were located in the proximal part of retinal arterioles close to the optic nerve (Figure 1B and 1C and Figure IA in the Data Supplement). Hence the three *CreERT2* lines labeled distinct and non-overlapping endothelial cell populations at this time point.

24 h and 48 h after injection, *Mfsd2a*-positive cells were progressively colonized the arteries from the distal to the proximal part (Figure 1D and 1G). *Esm1*-positive cells were seen at the tip position and moving towards the distal parts of the arterioles at 24 h and 48 h after injection (Figure 1E and 1H), while *Bmx*-positive cells remained confined to the proximal arterioles (Figure 1F and 1I and Figure IA in the Data Supplement). Very few *Mfsd2a*-GFP positive cells were detected in arteries 4 h and 6 h post Tx injection (Figure IB in the Data Supplement and Figure 1J), while 400 h after P4 Tx injection, ie at P21, most of the retinal endothelium was GFP-positive (Figure 1K). By contrast, a single Tx injection at P20 labeled venous and capillary endothelium, but not arteries at P21 (Figure 1L), demonstrating that ECs of venous and capillary origin migrate against the direction of flow into neighboring arteries during vascular remodeling. To test the requirement of blood flow as a driver for the migration of the *Mfsd2a*-GFP positive cells, we injected Tx to P5 *Mfsd2a Cre^{ERT2}* mice for 12 h, then isolated the retinas and cultured them for another 12 h, which reduced arterial colonization by GFP-positive cells (Figure IC in the Data Supplement). To quantify displacement of *Msfd2a*-GFP positive cells, we measured the relative length of GFP-positive area in retinal arteries, veins and capillaries at different time points (Figure 1M). After 12 h, about 90% of venous and capillary vessel area was occupied by GFP-positive cells, while only 50% of the distal arterial vessel area was occupied by GFP-positive cells and this gradually increased over time until 48 h (Figure 1M), demonstrating quantifiable displacement of capillary and venous ECs towards arteries over time.

Alk1 deletion in capillary and venous ECs causes AVMs

To determine the origin of AVM forming cells in *Alk1* mutants, we next intercrossed *Mfsd2a*, *Esm1* and *Bmx Cre^{ERT2}* mice with *Alk1$^{f/f}$ mTmG* reporter mice. Tx was injected at P4 and mice were analyzed at P6 (Figure 2A). Efficient *Alk1* deletion was verified in all three lines using immunostaining (Figure IIA–P in the Data Supplement). Interestingly, venous and capillary endothelial *Alk1* deletion using the *Mfsd2a Cre^{ERT2}* driver line led to numerous AVMs in the retina (Figure 2B and 2E). By contrast, neither *Alk1$^{f/f}$ Esm1 Cre^{ERT2}* nor *Alk1$^{f/f}$ Bmx Cre^{ERT2}* mutants displayed any retinal AVMs (Figure 2C–2E). We analyzed the presence of retinal and brain AVMs by injection of latex dye into the left ventricle of P6 *Alk1$^{f/f}$ Mfsd2a Cre^{ERT2}* and control littermates (Figure 2F–2I). The latex dye does not cross the capillary beds and was retained within the arterial branches in *Alk1$^{f/f}$* brain and retina (Figure 2F and 2G). In the *Alk1$^{f/f}$ Mfsd2a Cre^{ERT2}* mutants, the latex penetrated both the venous as well as the arterial branches via AVMs in the retina and brain (Figure 2H and 2I). To see whether *Alk1$^{f/f}$ Esm1 Cre^{ERT2}* and *Alk1$^{f/f}$ Bmx Cre^{ERT2}* could develop AVMs by longer-term exposure of Tx, Tx was injected at P1 and mice were analyzed at P6 (Figure IIQ in the Data Supplement). Neither *Alk1$^{f/f}$ Esm1 Cre^{ERT2}*

nor *Alk1*$^{f/f}$ *Bmx Cre*^{ERT2} mutants exhibited any AVMs (Figure IIR and IIS in the Data Supplement).

Next, we examined the survival rate of these three mouse lines. *Alk1*$^{f/f}$ *Mfsd2a Cre*^{ERT2} mice died 5–6 days after gene deletion, most likely from ruptured brain AVMs, while *Alk1*$^{f/f}$ *Bmx Cre*^{ERT2} mice lived at least 50 days after gene deletion (Figure IIT in the Data Supplement). Interestingly, the *Alk1*$^{f/f}$ *Esm1 Cre*^{ERT2} mutants died 10–11 days after Tx injection (Figure IIT in the Data Supplement), suggesting they might develop AVMs in other tissues. Autopsy revealed massive intestinal hemorrhages in *Alk1*$^{f/f}$ *Esm1 Cre*^{ERT2} mice as a likely cause of death (Figure IIU in the Data Supplement). To define the *Esm1* expression in intestines, Tx was injected at P4 and *Esm1 Cre*^{ERT2} *mTmG* mice were analyzed at P14. GFP-positive cells were found in scattered capillaries of the mesenteries, the intestinal wall and the intestinal villi (Figure 2J and 2K). We performed immunostaining of VE-Cadherin (VE-Cad) and GFP in P14 *Alk1*$^{f/f}$ and *Alk1*$^{f/f}$ *Esm1 Cre*^{ERT2} *mTmG* mice (Figure 2L and 2M). *Alk1*$^{f/f}$ *Esm1 Cre*^{ERT2} *mTmG* developed GFP-positive vascular malformations in capillaries of the intestinal villi (Figure 2M). Injection of latex dye confirmed the presence of AVMs in the intestinal villi and in the mesenteries (Figure 2N–2Q). To identify the presence of AVMs in other vascular beds, immunostaining and latex red dye injections were performed in P12 and P14 *Esm1 Cre*^{ERT2} *mTmG*, *Alk1*$^{f/f}$ and *Alk1*$^{f/f}$ *Esm1 Cre*^{ERT2} *(mTmG)* mice (Figure 2R–2W). *Alk1*$^{f/f}$ *Esm1 Cre*^{ERT2} *mTmG* developed GFP-positive vascular malformations in retinal capillaries, and migration of *Alk1* mutant tip cell progeny into the arteries was perturbed (Figure 2R and 2S). Latex injection confirmed abnormal patterning of distal retinal arteries derived from the *Esm1*-positive tip cells (Figure 2T and 2U). The latex also revealed vascular malformations in the pial arteries of the brain in *Alk1*$^{f/f}$ *Esm1 Cre*^{ERT2} mice (Figure 2V and 2W), but full-blown AVMs were not observed in retina or brain. These data indicate that loss of ALK1 signaling in ESM1 expressing capillaries leads to intestinal vascular malformations.

Loss of ALK1 affects cell polarity and flow-migration coupling.

To test if flow-mediated EC polarization was altered in the absence of ALK1, we dissected retinas at P6 −48 h after Tx injection- and immunolabeled with IB4 to detect ECs, DAPI to label nuclei, the Golgi marker GOLPH4 and ALK1 (Figure 3A–3F). To analyze the orientation of the Golgi toward the flow direction in the retinal vessels, we measured the angles between the EC nuclei and the Golgi as well as the predicted blood flow vectors (Figure 3C'–3F' and Figure 3G). In *Alk1*$^{f/f}$ retinas, ALK1 expressing arterial, venous and capillary ECs polarized against the direction of blood flow (Figure 3A, 3C, 3C' and 3H). In contrast, ECs from *Alk1*$^{f/f}$ *Mfsd2a Cre*^{ERT2} retinas showed random Golgi distribution in veins, capillaries and AVMs (Figure 3B, 3E, 3E', 3F, 3F' and 3H). ECs in proximal arteries of *Alk1*$^{f/f}$ *Mfsd2a Cre*^{ERT2} retinas where Cre was not active maintained ALK1 expression and were polarized normally against the flow (Figure 3B, 3D, 3D' and 3H). Quantification of polarization using a polarity index (PI), which ranges from 1 (strongly polarized) to 0 (random distribution) confirmed that *Alk1*$^{f/f}$ retinal ECs were strongly polarized against the direction of blood flow, while *Alk1*$^{f/f}$ *Mfsd2a Cre*^{ERT2} mutant ECs in capillaries, veins and AVMs displayed poor polarization against the direction of blood flow (Figure 3I). To determine whether the polarity defects preceded AVM development, Tx was injected

at P4 and *Alk1*$^{f/f}$ *Mfsd2a Cre*^{ERT2} mice were analyzed after 24 h (P5) or 36 h (P5.5). Interestingly, AVMs started to appear at 24 h and were more pronounced at 36 h (Figure 3J and 3K). Analysis of cell polarity in P5 *Alk1*$^{f/f}$ *Mfsd2a Cre*^{ERT2} mutants and controls showed that venous and capillary ECs from *Alk1*$^{f/f}$ *Mfsd2a Cre*^{ERT2} retinas displayed poorly polarized Golgi distribution (Figure 3L and 3M), indicating that lack of flow-induced polarity preceded AVM formation and could be causally related to AVM development.

To explore whether laminar flow affected the polarization of *ALK1* mutant cells *in vitro*, we performed scratch wound assays with human umbilical vein endothelial cells (HUVECs) that were cultured in static conditions or subjected to laminar shear stress (15 dynes/cm^2) and stained with a Golgi marker to determine cell polarity angles[29]. In static conditions, control siRNA transfected HUVECs were polarized towards the scratch areas in both the left and the right side of the wound (Figure 4A and 4C). Under laminar shear, the cells on the left side upstream of the scratch repolarize in the opposite direction to align against the flow (Figure 4E and 4G). By contrast, *ALK1* deficient HUVECs showed random polarization in static conditions (Figure 4B and 4D). Most strikingly, they were unable to polarize against the direction of flow in the upstream scratch areas, and even the downstream polarization against the flow was impaired (Figure 4F and 4H). Polarity index calculation showed that flow significantly enhanced polarization of control siRNA transfected cells, and that *ALK1* deletion prevented flow induced polarization (Figure 4I).

Flow induces localization of phosphorylated AKT to the upstream edge of ECs[30]. Pleckstrin homology domain of AKT fused to GFP (PH-AKT-GFP) is a well-established biosensor of PI3K local activity which shows plasma membrane localized PH-AKT-GFP upon shear stress[31]. To examine whether ALK1 affected flow-induced PI3K localization, we performed live cell imaging. PH-AKT-mClover3 together with plasma membrane marker (LCK-mRuby3) were co-expressed as a biosensor and an internal control respectively. Control siRNA transfected HUVECs showed polarized activation of PI3K on their upstream edge within 5 minutes after flow, consistent with upstream Golgi polarization. By contrast, *ALK1* knockdown significantly diminished this effect (Figure 4J, 4K and Movie I in the Data Supplement). This result indicated that ALK1 is required for flow-induced PI3K-AKT polarization.

Blockade of integrin prevents AVM formation.

Golgi orientation into scratch wounds and under flow is driven by integrin binding to ECM proteins and signaling to CDC42[32, 33]. Additionally, integrin activation and signaling is modulated by VEGFR2-PI3K signaling, which is altered following ALK1 deletion[12, 13, 1834]. VEGFR2 interacts with integrins $\alpha_v\beta_3$ and $\alpha_5\beta_1$ during vascularization[35–37], prompting us to test if VEGFR2-integrin signaling was enhanced in ALK1 deficient ECs. Interestingly, immunolabeling with antibodies recognizing integrin β1 (ITGB1), α5 (ITGA5) and αv (ITGAV) showed increased ITGB1, ITGA5 and ITGAV expression in the AVM areas of P8 *Alk1*$^{f/f}$ *Mfsd2a Cre*^{ERT2} retinas when compared to wildtype controls (Figure 5A–5D and Figure IIIA–IIIC in the Data Supplement). We next tested if *ALK1* knockdown affected VEGFR2 complex formation with integrins. VEGFR2 immunoprecipitation and immunoblotting for integrins showed that *ALK1*

deletion significantly enhanced VEGFR2 pulldown of ITGB1, ITGA5 and ITGAV, and that *VEGFR2* knockdown abolished co-immunoprecipitation, without affecting total levels of ITGB1, ITGA5 and ITGAV in cell lysates (Figure 5E, 5F and Figure IIID in the Data Supplement). These results suggested that targeting integrin signaling with inhibitors could rescue AVM formation. To test this idea, we administered cilengitide, a small molecule inhibitor for integrin $\alpha_v\beta_3$ and $\alpha_v\beta_5$, or ATN161, a peptide inhibitor for integrin $\alpha_5\beta_1$. *Alk1* deletion was induced by Tx injection at P4, inhibitors were given intraperitoneally (i.p.) at 5 mg/kg at P4 and P5, and mice were analyzed at P6 (Figure 5G). Both cilengitide and ATN161 decreased AVM formation in *Alk1*$^{f/f}$ *Mfsd2a Cre*^{ERT2} or *Alk1*$^{f/f}$ *Cdh5 Cre*^{ERT2} mice (Figure 5H–5O). Immunostaining of Golgi markers showed that integrin inhibitors rescued polarization of *Alk1* mutant cells against the direction of blood flow (Figure 5P–5T).

ALK1 controls Hippo pathway signaling.

Previous data reported an interaction between BMP9/ALK1 signaling and the YAP/TAZ pathway, and both of these pathways are regulated by blood flow *in vivo*[38, 39]. Moreover, integrins are potent regulators of YAP/TAZ activation in many systems including ECs[40–42]. To test whether laminar shear and ALK1 affected integrin and YAP/TAZ protein expression, HUVECs were transfected with control or *ALK1* siRNA and cultured in static conditions or under laminar shear stress (15 dynes/cm^2) for 18 h. Protein extracts from these cells were analyzed by western blot with antibodies against integrins, YAP or TAZ and expression levels were compared to β-ACTIN. Interestingly, ITGB1, ITGA5 and ITGAV as well as YAP and TAZ were all significantly increased in *ALK1* deleted ECs when compared to control siRNA transfected cells, and their expression was further increased by laminar shear stress (Figure 6A and 6B). YAP and TAZ protein expression were also increased and appeared more nuclear in *Alk1*$^{f/f}$ *Mfsd2a Cre*^{ERT2} retina AVMs when compared to *Alk1*$^{f/f}$ control ECs (Figure 6C–6F). Immunostaining of HUVECs with YAP and TAZ antibodies revealed enhanced YAP and TAZ nuclear localization in *ALK1* deficient cells, while YAP and TAZ were mainly located in the cytosol of control siRNA treated ECs (Figure 6G and 6H). To test whether other HHT pathway components *ENG* and *SMAD4* also affected YAP/TAZ activity, we deleted *ALK1*, *SMAD4*, and *ENG* in HUVECs and immune-labeled for YAP and TAZ (Figure 7A). YAP and TAZ nuclear localization increased in *ALK1*, *SMAD4*, and *ENG* deleted ECs when compared to control siRNA transfected cells (Figure 7A and 7B). Treatment with the YAP/TAZ inhibitor Verteporfin (VP) blocked YAP/TAZ nuclear translocation in *ALK1*, *SMAD4*, and *ENG* depleted HUVECs (Figure 7A and 7B). *ALK1* deletion also increased expression of the YAP/TAZ target cMYC[43, 44] and enhanced cMYC nuclear localization. Nuclear cMYC expression was significantly reduced by VP treatment of *ALK1* knockdown cells (Figure IVA–IVD in the Data Supplement). To examine VP activity *in vivo*, we administered VP (50 mg/kg, i.p.) into P4 and P5 *Alk1*$^{f/f}$ control mice (Figure 7C). VP injected control retinas developed blunted endothelial tip cells at the angiogenic front (Figure 7D), as reported in genetically *Yap/Taz* deficient endothelial mouse retinas[38, 45, 46] indicating that the pharmacological inhibition was effective. Next, we injected VP into *Alk1*$^{f/f}$ *Cdh5 Cre*^{ERT2} or *Alk1*$^{f/f}$ *Mfsd2a Cre*^{ERT2} retinas, which led to a significant reduction of AVM formation and hemorrhage when compared to DMSO vehicle treated mutant retinas (Figure 7D–7F). VP treatment also rescued the polarization against

the direction of blood flow (Figure 7G and 7H). These results demonstrated that ALK1 regulates Hippo pathway activation, and that VP-mediated inhibition of YAP/TAZ activity improved flow migration coupling and prevented AVMs in *Alk1* mutant ECs.

VEGFR2, integrin and PI3K function upstream of YAP/TAZ in Alk1 mutants

To elucidate whether ALK1 modulation of the Hippo pathway was dependent on VEGFR2, integrins, and PI3K, we examined YAP/TAZ nuclear translocation by immunostaining. YAP/TAZ nuclear translocation was abolished by combined deletion of *ALK1* and *VEGFR2* (Figure 8A and 8B), by treating *ALK1* deleted HUVECs with integrin inhibitors cilengitide or ATN161, and by treatment with the PI3K inhibitor wortmannin (Figure 8A, 8B and Figure VA–VC in the Data Supplement). Western blot analysis showed that combined deletion of *ALK1* and *VEGFR2* and/or *ITGB1* reduced YAP/TAZ expression and phosphorylation of PI3K and AKT (Figure 8C and 8D), supporting that VEGFR2-integrin signaling through PI3K/AKT acts upstream of YAP/TAZ in *ALK1* deficient HUVECs. *Alk1* deletion in mouse brain ECs likewise revealed enhanced YAP/TAZ expression and enhanced PI3K/AKT phosphorylation, and this could be rescued by over-expression of *ALK1* (Figure VIA and VIB in the Data Supplement). *In vivo*, cilengitide and ATN161 treatment of $Alk1^{f/f}$ *Mfsd2a* Cre^{ERT2} mice reduced YAP/TAZ expression when compared to $Alk1^{f/f}$ control retinas (Figure 8E), supporting that integrin signaling acted upstream of YAP/TAZ.

Discussion

This study shows that AVMs in *Alk1* mutants originate from capillaries and veins and implicates integrin and Hippo pathway signaling in HHT. The data are consistent with a model whereby the presence of ALK1 suppresses integrin signaling interactions with VEGFR2, which limits PI3K activation and YAP/TAZ nuclear translocation. In the absence of ALK1, enhanced VEGFR2-integrin-PI3K signaling promotes YAP/TAZ nuclear translocation, and pharmacological inhibition of integrin or YAP/TAZ signaling prevents vascular malformations in *Alk1* deficient mice (Figure VII in the Data Supplement), as does VEGFR2 or PI3K inhibition[13, 20, 47, 48].

We found that *Mfsd2a*-positive capillary-venous cells migrated against the blood flow direction towards retinal arteries, highlighting endothelial flow-migration coupling as a critical process driving vascular remodeling[29, 49, 50]. The current concept suggests that blood flow attracts EC migration from low flow segments (veins and capillaries) towards high flow segments (arteries)[49]. Hence, disruption of flow-migration coupling and resulting accumulation of ECs in capillaries could cause capillary enlargement and thereby precipitate AVM formation. Consistent with this model, deletion of *Alk1* in capillaries and veins using *Mfsd2a* Cre^{ERT2} led to disruption of Golgi polarization against the flow direction and caused retinal and cerebral AVMs. Mfsd2a is a brain-specific endothelial gene[24, 51], hence our analysis of these mice was restricted to the brain and retina. In addition, a recent study showed that capillary/venous-specific deletion of the ALK1 co-receptor ENG using $Eng^{fl/fl}$ *Apj-*Cre^{ERT2} mice induced retinal AVMs[52], indicating that the ALK1-ENG complex is required in capillaries and veins to prevent AVM formation, and that defective flow-migration coupling is a hallmark of HHT. Whether venous or capillary ECs, or both,

are involved in the vascular malformations, needs to be further investigated and will require generation of capillary or vein-specific Cre driver lines.

Interestingly, deletion of *Alk1* in *Esm1*-positive tip cells also led to defective flow-migration coupling and accumulation of the mutant cells in the vascular plexus ahead of the arteries, while control cells colonized the arterial tree. This underscores an important role of *Alk1* in flow-migration coupling of retinal tip cells, but produced only mild retinal and brain vascular malformations when compared to pan-endothelial *Alk1*$^{f/f}$ *Cdh5 Cre*^{ERT2} and *Alk1*$^{f/f}$ *Mfsd2a Cre*^{ERT2} mice. One possible reason for the discrepant phenotypes is that disruption of cell polarity per se is not sufficient to induce AVMs. Another possibility is the differing flow environment: *Esm1*-positive tip cells migrate in a low-flow environment, whereas AVMs develop in high-flow regions of the retina, close to the optic nerve, and we and others have previously reported that blood flow potentiates ALK1-ENG-mediated shear stress sensing[15, 26].

Quite strikingly, despite the lack of AVMs in retina and brain, the *Alk1*$^{f/f}$ *Esm1 Cre*^{ERT2} mice developed intestinal AVMs and succumbed to intestinal hemorrhage. Analysis of *Esm1*-driven GFP labeling revealed expression in capillary endothelium of the mesenteries, the gut wall and the intestinal villi, and GFP positive cells formed AVMs in those regions in *Alk1*$^{f/f}$ *Esm1 Cre*^{ERT2} mutant mice. Hence, capillary function of *Alk1* was required to prevent intestinal AVM formation. Further analysis is required to assess whether flow-migration coupling also underlies intestinal vascular remodeling, but such studies will require endothelial specific fluorescent Golgi reporter mice to determine endothelial cell polarity.

Our *in vitro* data revealed that loss of ALK1 displayed disrupted endothelial Golgi orientation and polarization against the blood flow direction. Blocking blood flow in zebrafish *alk1* mutants prevented AVM formation, directly demonstrating that blood flow induces AVM formation in the absence of ALK1[53]. We and others have previously reported that BMP9/10-ALK1 signaling mechanistically links flow sensing and VEGFR2-PI3K/AKT pathway activation [12–15, 17, 20, 54]. ALK1 signaling counteracted both flow and growth factor-induced AKT activation, and the absence of ALK1 overactivated PI3K/AKT signaling in AVMs [48, 55, 56]. We extend these findings here by demonstrating that ALK1 is required for flow-induced PI3K-AKT polarization against the direction of blood flow. Besides enhanced VEGFR2/PI3K signaling, another study showed that loss of SMAD4 increased Angiopoietin2 and decreased TIE2 receptor expression[57]. Blocking Angiopoietin2 prevented AVM formation and normalized vessel diameters in endothelial *Smad4* deficient mice, while TIE2 accumulated within the AVMs[57], suggesting that increased TIE2 signaling could contribute to enhanced PI3K signaling in AVMs.

As new mechanistic findings, we report that integrins and YAP/TAZ signaling are involved in ALK1 signaling and AVM formation. Integrins are heterodimeric transmembrane receptors that are activated by flow and then bind to specific ECM proteins. RGD peptides or neutralizing antibodies against integrin $\alpha_5\beta_1$ prevented laminar shear stress-induced increase in EC adhesion[58–60]. This correlates with our data that *Alk1* mutant showed increased integrins in AVM regions and cilengitide and ATN161 improved AVMs in *Alk1*

mutant mice. Cilengitide is a selective $\alpha_v\beta_3$ and $\alpha_v\beta_5$ integrin inhibitor. Phase 3 trials using cilengitide for glioblastoma patients have failed to improve patient survival, however they were well tolerated[61] and could be viable candidates for therapy in HHT patients.

Hippo-YAP/TAZ signaling regulates organ size, tissue regeneration and self-renewal as well as vascular development[38, 39, 62–65]. The core components of this pathway comprise a kinase cascade containing MST1/2 and LATS1/2. MST1/2 phosphorylates and activates LATS1/2, which then phosphorylate YAP/TAZ, causing their cytoplasmic sequestration, degradation and inactivation[66, 67]. When activated, YAP/TAZ shuffle from the cytosol to the nucleus where they interact with different transcription factors, of which TEAD transcription factors are the best characterized, to regulate expression of target genes involved in cell growth, survival, and migration[68]. Endothelial YAP/TAZ are important regulators of vascular development and function, and their activity is regulated by mechanical, metabolic and growth factor signals[39, 45, 46, 62, 69–71]. We found that ALK1 deletion in mice or in human ECs induced nuclear YAP/TAZ accumulation in a VEGFR2, PI3K and integrin-dependent manner, thereby linking YAP/TAZ signaling to HHT. The mechanistic details of Hippo pathway regulation by ALK1 remain to be determined. VEGFR2 signaling triggers integrin activation through PI3K[72–74], alternatively PI3K can be activated downstream of VEGFR2 and integrins through outside-in signaling[74–77]. Because ITGB1 knockdown decreased PI3K activation in ALK1 knockdown cells, our data favor the latter model. Integrins are well known to activate YAP/TAZ through both mechanical and biochemical signaling pathways[78, 79]. Together, these results define a pathway in which loss of ALK1 activates VEGFR2-integrin and PI3K, which, in turn, activates YAP/TAZ. However, as nuclear YAP/TAZ accumulation alone is not reported to induce AVMs[65, 80], we suggest that YAP/TAZ are necessary but not sufficient for AVM formation, and that VEGFR2, PI3K and integrins very likely contribute to lesion formation through additional effects on cell polarity and migration. Finally, YAP/TAZ overactivation suppressed BMP9-ALK1 signaling[38], suggesting that negative feedback loops between these pathways occur during normal vascular development. We show that the YAP/TAZ inhibitor VP, which inhibits YAP/TAZ translocation to the nucleus[81, 82] and blocks YAP-TEAD association by binding to YAP and changing its conformation[83], rescued AVM formation in *Alk1* mutant mice. VP photodynamic therapy is approved for the treatment of choroidal neovascularization due to age-related macular degeneration[84] and both integrin inhibitors and verteporfin might be novel therapeutic options for HHT patients.

Supplementary Material

Refer to Web version on PubMed Central for supplementary material.

Acknowledgements

We thank ATTRACT members Paul Oh, Lena Claesson-Welsh, Miguel Bernabeu and Holger Gerhardt for critical comments on the manuscript, Profs Bin Zhou (Shanghai Institute for Biological Sciences) and Ralf Adams (Max-Planck Institute, Munster, Germany) for mouse lines, and Dr. Jihoon Park for Python scripts to measure polarity and index.

Sources of Funding

This work was supported by grants from the Leducq Foundation (TNE ATTRACT, A.E, C.F) and NIH (P30 EY026878, R01EY025979 to A.E and R01 HL135582 to M.A.S). C.A.F was supported by European Research Council starting grant (679368) and the Fundação para a Ciência e a Tecnologia funding (CEECIND/02589/2018).

Non-standard Abbreviations and Acronyms

AVMs	arteriovenous malformations
GI	Gastrointestinal
HHT	Hereditary hemorrhagic telangiectasia
HUVECs	human umbilical vein endothelial cells
i.p.	intraperitoneally
LSS	laminar shear stress
PI	Polarity index
SEM	Standard error of the mean
Tx	Tamoxifen

References

1. Shovlin CL. Hereditary haemorrhagic telangiectasia: Pathophysiology, diagnosis and treatment. Blood Reviews. 2010;24:203–219. doi: 10.1016/j.blre.2010.07.001 [PubMed: 20870325]
2. McAllister KA, Grogg KM, Johnson DW, Gallione CJ, Baldwin MA, Jackson CE, Helmbold EA, Markel DS, McKinnon WC, Murrel J, et al.Endoglin, a TGF-β binding protein of endothelial cells, is the gene for hereditary haemorrhagic telangiectasia type 1. Nature Genetics. 1994;8:345–351. doi: 10.1038/ng1294-345 [PubMed: 7894484]
3. Johnson DW, Berg JN, Baldwin MA, Gallione CJ, Marondel I, Yoon SJ, Stenzel TT, Speer M, Pericak-Vance MA, Diamond A, et al.Mutations in the activin receptor–like kinase 1 gene in hereditary haemorrhagic telangiectasia type 2. Nature Genetics. 1996;13:189–195. doi: 10.1038/ng0696-189 [PubMed: 8640225]
4. Gallione CJ, Repetto GM, Legius E, Rustgi AK, Schelley SL, Tejpar S, Mitchell G, Drouin E, Westermann CJ and Marchuk DA. A combined syndrome of juvenile polyposis and hereditary haemorrhagic telangiectasia associated with mutations in MADH4 (SMAD4). Lancet. 2004;363:852–9. doi: 10.1016/s0140-6736(04)15732-2 [PubMed: 15031030]
5. Gallione CJ, Klaus DJ, Yeh EY, Stenzel TT, Xue Y, Anthony KB, McAllister KA, Baldwin MA, Berg JN, Lux A, et al.Mutation and expression analysis of the endoglin gene in Hereditary Hemorrhagic Telangiectasia reveals null alleles. Human Mutation. 1998;11:286–294. doi: 10.1002/(SICI)1098-1004(1998)11:4<286::AID-HUMU6>3.0.CO;2-B [PubMed: 9554745]
6. Roman BL and Hinck AP. ALK1 signaling in development and disease: new paradigms. Cellular and Molecular Life Sciences. 2017;74:4539–4560. doi: 10.1007/s00018-017-2636-4 [PubMed: 28871312]
7. David L, Mallet C, Mazerbourg S, Feige JJ and Bailly S. Identification of BMP9 and BMP10 as functional activators of the orphan activin receptor-like kinase 1 (ALK1) in endothelial cells. Blood. 2007;109:1953–61. doi: 10.1182/blood-2006-07-034124 [PubMed: 17068149]
8. Ruiz-Llorente L, Gallardo-Vara E, Rossi E, Smadja DM, Botella LM and Bernabeu C. Endoglin and alk1 as therapeutic targets for hereditary hemorrhagic telangiectasia. Expert Opinion on Therapeutic Targets. 2017;21:933–947. doi: 10.1080/14728222.2017.1365839 [PubMed: 28796572]
9. Snellings DA, Gallione CJ, Clark DS, Vozoris NT, Faughnan ME and Marchuk DA. Somatic Mutations in Vascular Malformations of Hereditary Hemorrhagic Telangiectasia Result in Bi-allelic

Loss of ENG or ACVRL1. American Journal of Human Genetics. 2019;105:894–906. doi: 10.1016/j.ajhg.2019.09.010 [PubMed: 31630786]

10. Govani FS and Shovlin CL. Hereditary haemorrhagic telangiectasia: A clinical and scientific review. European Journal of Human Genetics. 2009;17:860–871. doi: 10.1038/ejhg.2009.35 [PubMed: 19337313]
11. McDonald J, Bayrak-Toydemir P and Pyeritz RE. Hereditary hemorrhagic telangiectasia: An overview of diagnosis, management, and pathogenesis. Genetics in Medicine. 2011;13:607–616. doi: 10.1097/GIM.0b013e3182136d32 [PubMed: 21546842]
12. Tual-Chalot S, Mahmoud M, Allinson KR, Redgrave RE, Zhai Z, Oh SP, Fruttiger M and Arthur HM. Endothelial depletion of Acvrl1 in mice leads to arteriovenous malformations associated with reduced endoglin expression. PLoS One. 2014;9:e98646. doi: 10.1371/journal.pone.0098646
13. Ola R, Dubrac A, Han J, Zhang F, Fang JS, Larrivée B, Lee M, Urarte AA, Kraehling JR, Genet G, et al.PI3 kinase inhibition improves vascular malformations in mouse models of hereditary haemorrhagic telangiectasia. Nature Communications. 2016;7:13650. doi: 10.1038/ncomms13650
14. Ola R, Künzel Sandrine H, Zhang F, Genet G, Chakraborty R, Pibouin-Fragner L, Martin K, Sessa W, Dubrac A and Eichmann A. SMAD4 Prevents Flow Induced Arteriovenous Malformations by Inhibiting Casein Kinase 2. Circulation. 2018;138:2379–2394. doi: 10.1161/CIRCULATIONAHA.118.033842 [PubMed: 29976569]
15. Baeyens N, Larrivée B, Ola R, Hayward-Piatkowskyi B, Dubrac A, Huang B, Ross TD, Coon BG, Min E, Tsarfati M, et al.Defective fluid shear stress mechanotransduction mediates hereditary hemorrhagic telangiectasia. The Journal of Cell Biology. 2016;214:807. doi: 10.1083/jcb.201603106 [PubMed: 27646277]
16. Capasso TL, Li B, Volek HJ, Khalid W, Rochon ER, Anbalagan A, Herdman C, Yost HJ, Villanueva FS, Kim K, et al.BMP10-mediated ALK1 signaling is continuously required for vascular development and maintenance. Angiogenesis. 2020;23:203–220. doi: 10.1007/s10456-019-09701-0 [PubMed: 31828546]
17. Rochon ER, Menon PG and Roman BL. Alk1 controls arterial endothelial cell migration in lumenized vessels. Development. 2016;143:2593–602. doi: 10.1242/dev.135392 [PubMed: 27287800]
18. Han C, Choe S-w, Kim YH, Acharya AP, Keselowsky BG, Sorg BS, Lee Y-J and Oh SP. VEGF neutralization can prevent and normalize arteriovenous malformations in an animal model for hereditary hemorrhagic telangiectasia 2. Angiogenesis. 2014;17:823–830. doi: 10.1007/s10456-014-9436-3 [PubMed: 24957885]
19. Jin Y, Muhl L, Burmakin M, Wang Y, Duchez AC, Betsholtz C, Arthur HM and Jakobsson L. Endoglin prevents vascular malformation by regulating flow-induced cell migration and specification through VEGFR2 signalling. Nature Cell Biology. 2017;19:639–652. doi: 10.1038/ncb3534 [PubMed: 28530660]
20. Alsina-Sanchís E, García-Ibáñez Y, Figueiredo AM, Riera-Domingo C, Figueras A, Matias-Guiu X, Casanovas O, Botella LM, Pujana MA, Riera-Mestre A, et al.ALK1 Loss Results in Vascular Hyperplasia in Mice and Humans Through PI3K Activation. Arterioscler Thromb Vasc Biol. 2018;38:1216–1229. doi: 10.1161/atvbaha.118.310760 [PubMed: 29449337]
21. Iriarte A, Figueras A, Cerdà P, Mora JM, Jucglà A, Penín R, Viñals F and Riera-Mestre A. PI3K (Phosphatidylinositol 3-Kinase) Activation and Endothelial Cell Proliferation in Patients with Hemorrhagic Hereditary Telangiectasia Type 1. Cells. 2019;8. doi: 10.3390/cells8090971
22. Pu W, Zhang H, Huang X, Tian X, He L, Wang Y, Zhang L, Liu Q, Li Y, Li Y, et al.Mfsd2a+ hepatocytes repopulate the liver during injury and regeneration. Nat Commun. 2016;7:13369. doi: 10.1038/ncomms13369 [PubMed: 27857132]
23. Pu W, He L, Han X, Tian X, Li Y, Zhang H, Liu Q, Huang X, Zhang L, Wang QD, et al.Genetic Targeting of Organ-Specific Blood Vessels. Circ Res. 2018;123:86–99. doi: 10.1161/circresaha.118.312981 [PubMed: 29764841]
24. Chow BW, Nuñez V, Kaplan L, Granger AJ, Bistrong K, Zucker HL, Kumar P, Sabatini BL and Gu C. Caveolae in CNS arterioles mediate neurovascular coupling. Nature. 2020;579:106–110. doi: 10.1038/s41586-020-2026-1 [PubMed: 32076269]

25. Pitulescu ME, Schmidt I, Giaimo BD, Antoine T, Berkenfeld F, Ferrante F, Park H, Ehling M, Biljes D, Rocha SF, et al.Dll4 and Notch signalling couples sprouting angiogenesis and artery formation. Nature Cell Biology. 2017;19:915. doi: 10.1038/ncb3555 [PubMed: 28714968]
26. Xu C, Hasan SS, Schmidt I, Rocha SF, Pitulescu ME, Bussmann J, Meyen D, Raz E, Adams RH and Siekmann AF. Arteries are formed by vein-derived endothelial tip cells. Nature Communications. 2014;5:5758. doi: 10.1038/ncomms6758
27. Ehling M, Adams S, Benedito R and Adams RH. Notch controls retinal blood vessel maturation and quiescence. Development. 2013;140:3051. doi: 10.1242/dev.093351 [PubMed: 23785053]
28. Muzumdar MD, Tasic B, Miyamichi K, Li L and Luo L. A global double-fluorescent Cre reporter mouse. Genesis. 2007;45:593–605. doi: 10.1002/dvg.20335 [PubMed: 17868096]
29. Carvalho JR, Fortunato IC, Fonseca CG, Pezzarossa A, Barbacena P, Dominguez-Cejudo MA, Vasconcelos FF, Santos NC, Carvalho FA and Franco CA. Non-canonical Wnt signaling regulates junctional mechanocoupling during angiogenic collective cell migration. eLife. 2019;8:e45853. doi: 10.7554/eLife.45853
30. Melchior B and Frangos JA. Distinctive subcellular Akt-1 responses to shear stress in endothelial cells. Journal of Cellular Biochemistry. 2014;115:121–129. doi: 10.1002/jcb.24639 [PubMed: 23913776]
31. Várnai P and Balla T. Visualization of phosphoinositides that bind pleckstrin homology domains: Calcium- and agonist-induced dynamic changes and relationship to myo-[3H]inositol-labeled phosphoinositide pools. Journal of Cell Biology. 1998;143:501–510. doi: 10.1083/jcb.143.2.501
32. Etienne-Manneville S and Hall A. Integrin-mediated activation of Cdc42 controls cell polarity in migrating astrocytes through PKCzeta. Cell. 2001;106:489–98. doi: 10.1016/s0092-8674(01)00471-8 [PubMed: 11525734]
33. Tzima E, Kiosses WB, del Pozo MA and Schwartz MA. Localized cdc42 activation, detected using a novel assay, mediates microtubule organizing center positioning in endothelial cells in response to fluid shear stress. J Biol Chem. 2003;278:31020–3. doi: 10.1074/jbc.M301179200 [PubMed: 12754216]
34. Tzima E, Irani-Tehrani M, Kiosses WB, Dejana E, Schultz DA, Engelhardt B, Cao G, DeLisser H and Schwartz MA. A mechanosensory complex that mediates the endothelial cell response to fluid shear stress. Nature. 2005;437:426–31. doi: 10.1038/nature03952 [PubMed: 16163360]
35. Somanath PR, Malinin NL and Byzova TV. Cooperation between integrin αvβ3 and VEGFR2 in angiogenesis. Angiogenesis. 2009;12:177–185. doi: 10.1007/s10456-009-9141-9 [PubMed: 19267251]
36. Simons M. An inside view: VEGF receptor trafficking and signaling. Physiology (Bethesda). 2012;27:213–22. doi: 10.1152/physiol.00016.2012 [PubMed: 22875452]
37. Serini G, Napione L, Arese M and Bussolino F. Besides adhesion: new perspectives of integrin functions in angiogenesis. Cardiovascular Research. 2008;78:213–222. doi: 10.1093/cvr/cvn045 [PubMed: 18285512]
38. Neto F, Klaus-Bergmann A, Ong YT, Alt S, Vion A-C, Szymborska A, Carvalho JR, Hollfinger I, Bartels-Klein E, Franco CA, et al.YAP and TAZ regulate adherens junction dynamics and endothelial cell distribution during vascular development. eLife. 2018;7:e31037. doi: 10.7554/eLife.31037
39. Nakajima H, Yamamoto K, Agarwala S, Terai K, Fukui H, Fukuhara S, Ando K, Miyazaki T, Yokota Y, Schmelzer E, et al.Flow-Dependent Endothelial YAP Regulation Contributes to Vessel Maintenance. Developmental Cell. 2017;40:523–536.e6. doi: 10.1016/j.devcel.2017.02.019 [PubMed: 28350986]
40. Wang L, Luo JY, Li B, Tian XY, Chen LJ, Huang Y, Liu J, Deng D, Lau CW, Wan S, et al.Integrin-YAP/TAZ-JNK cascade mediates atheroprotective effect of unidirectional shear flow. Nature. 2016;540:579–582. doi: 10.1038/nature20602 [PubMed: 27926730]
41. Li B, He J, Lv H, Liu Y, Lv X, Zhang C, Zhu Y and Ai D. c-Abl regulates YAPY357 phosphorylation to activate endothelial atherogenic responses to disturbed flow. J Clin Invest. 2019;129:1167–1179. doi: 10.1172/jci122440 [PubMed: 30629551]

42. Dupont S. Role of YAP/TAZ in cell-matrix adhesion-mediated signalling and mechanotransduction. Exp Cell Res. 2016;343:42–53. doi: 10.1016/j.yexcr.2015.10.034 [PubMed: 26524510]
43. Choi W, Kim J, Park J, Lee DH, Hwang D, Kim JH, Ashktorab H, Smoot D, Kim SY, Choi C, et al.YAP/TAZ Initiates Gastric Tumorigenesis via Upregulation of MYC. Cancer Res. 2018;78:3306–3320. doi: 10.1158/0008-5472.Can-17-3487 [PubMed: 29669762]
44. Yamaguchi H and Taouk GM. A Potential Role of YAP/TAZ in the Interplay Between Metastasis and Metabolic Alterations. Frontiers in Oncology. 2020;10. doi: 10.3389/fonc.2020.00928
45. Sakabe M, Fan J, Odaka Y, Liu N, Hassan A, Duan X, Stump P, Byerly L, Donaldson M, Hao J, et al.YAP/TAZ-CDC42 signaling regulates vascular tip cell migration. Proc Natl Acad Sci U S A. 2017;114:10918–10923. doi: 10.1073/pnas.1704030114 [PubMed: 28973878]
46. Kim J, Kim YH, Kim J, Park DY, Bae H, Lee DH, Kim KH, Hong SP, Jang SP, Kubota Y, et al.YAP/TAZ regulates sprouting angiogenesis and vascular barrier maturation. J Clin Invest. 2017;127:3441–3461. doi: 10.1172/jci93825 [PubMed: 28805663]
47. Kim YH, Kim MJ, Choe SW, Sprecher D, Lee YJ and S PO. Selective effects of oral antiangiogenic tyrosine kinase inhibitors on an animal model of hereditary hemorrhagic telangiectasia. J Thromb Haemost. 2017;15:1095–1102. doi: 10.1111/jth.13683 [PubMed: 28339142]
48. Ruiz S, Zhao H, Chandakkar P, Papoin J, Choi H, Nomura-Kitabayashi A, Patel R, Gillen M, Diao L, Chatterjee PK, et al.Correcting Smad1/5/8, mTOR, and VEGFR2 treats pathology in hereditary hemorrhagic telangiectasia models. Journal of Clinical Investigation. 2020;130:942–957. doi: 10.1172/JCI127425
49. Franco CA, Jones ML, Bernabeu MO, Geudens I, Mathivet T, Rosa A, Lopes FM, Lima AP, Ragab A, Collins RT, et al.Dynamic Endothelial Cell Rearrangements Drive Developmental Vessel Regression. PLOS Biology. 2015;13:e1002125. doi: 10.1371/journal.pbio.1002125
50. Fonseca CG, Barbacena P and Franco CA. Endothelial cells on the move: dynamics in vascular morphogenesis and disease. Vasc Biol. 2020;2:H29–h43. doi: 10.1530/vb-20-0007 [PubMed: 32935077]
51. Chow BW and Gu C. Gradual Suppression of Transcytosis Governs Functional Blood-Retinal Barrier Formation. Neuron. 2017;93:1325–1333.e3. doi: 10.1016/j.neuron.2017.02.043
52. Singh E, Redgrave RE, Phillips HM and Arthur HM. Arterial endoglin does not protect against arteriovenous malformations. Angiogenesis. 2020;23:559–566. doi: 10.1007/s10456-020-09731-z [PubMed: 32506200]
53. Corti P, Young S, Chen CY, Patrick MJ, Rochon ER, Pekkan K and Roman BL. Interaction between alk1 and blood flow in the development of arteriovenous malformations. Development. 2011;138:1573–82. doi: 10.1242/dev.060467 [PubMed: 21389051]
54. Tual-Chalot S, Garcia-Collado M, Redgrave RE, Singh E, Davison B, Park C, Lin H, Luli S, Jin Y, Wang Y, et al.Loss of endothelial endoglin promotes high-output heart failure through peripheral arteriovenous shunting driven by VEGF signaling. Circulation Research. 2020:243–257. doi: 10.1161/CIRCRESAHA.119.315974 [PubMed: 31805812]
55. Thalgott JH, Dos-Santos-Luis D, Hosman AE, Martin S, Lamandé N, Bracquart D, Srun S, Galaris G, De Boer HC, Tual-Chalot S, et al.Decreased expression of vascular endothelial growth factor receptor 1 contributes to the pathogenesis of hereditary hemorrhagic telangiectasia type 2. Circulation. 2018;138:2698–2712. doi: 10.1161/CIRCULATIONAHA.117.033062 [PubMed: 30571259]
56. Hwan Kim Y, Vu PN, Choe SW, Jeon CJ, Arthur HM, Vary CPH, Lee YJ and Oh SP. Overexpression of Activin Receptor-Like Kinase 1 in Endothelial Cells Suppresses Development of Arteriovenous Malformations in Mouse Models of Hereditary Hemorrhagic Telangiectasia. Circ Res. 2020;127:1122–1137. doi: 10.1161/circresaha.119.316267 [PubMed: 32762495]
57. Crist AM, Zhou X, Garai J, Lee AR, Thoele J, Ullmer C, Klein C, Zabaleta J and Meadows SM. Angiopoietin-2 Inhibition Rescues Arteriovenous Malformation in a Smad4 Hereditary Hemorrhagic Telangiectasia Mouse Model. Circulation. 2019;139:2049–2063. doi: 10.1161/CIRCULATIONAHA.118.036952 [PubMed: 30744395]

58. Xanthis I, Souilhol C, Serbanovic-Canic J, Roddie H, Kalli AC, Fragiadaki M, Wong R, Shah DR, Askari JA, Canham L, et al.β1 integrin is a sensor of blood flow direction. Journal of Cell Science. 2019;132(11). doi: 10.1242/JCS.229542
59. Urbich C, Walter DH, Zeiher AM and Dimmeler S. Laminar shear stress upregulates integrin expression role in endothelial cell adhesion and apoptosis. Circulation Research. 2000;87:683–689. doi: 10.1161/01.RES.87.8.683 [PubMed: 11029404]
60. Tzima E, Del Pozo MA, Shattil SJ, Chien S and Schwartz MA. Activation of integrins in endothelial cells by fluid shear stress mediates Rho-dependent cytoskeletal alignment. EMBO Journal. 2001;20:4639–4647. doi: 10.1093/emboj/20.17.4639
61. Stupp R, Hegi ME, Gorlia T, Erridge SC, Perry J, Hong YK, Aldape KD, Lhermitte B, Pietsch T, Grujicic D, et al.Cilengitide combined with standard treatment for patients with newly diagnosed glioblastoma with methylated MGMT promoter (CENTRIC EORTC 26071–22072 study): a multicentre, randomised, open-label, phase 3 trial. The Lancet Oncology. 2014;15:1100–1108. doi: 10.1016/S1470-2045(14)70379-1 [PubMed: 25163906]
62. Wang X, Freire Valls A, Schermann G, Shen Y, Moya IM, Castro L, Urban S, Solecki GM, Winkler F, Riedemann L, et al.YAP/TAZ Orchestrate VEGF Signaling during Developmental Angiogenesis. Developmental Cell. 2017;42:462–478.e7. doi: 10.1016/j.devcel.2017.08.002 [PubMed: 28867486]
63. Wang K-C, Yeh Y-T, Nguyen P, Limqueco E, Lopez J, Thorossian S, Guan K-L, Li Y-SJ and Chien S. Flow-dependent YAP/TAZ activities regulate endothelial phenotypes and atherosclerosis. Proceedings of the National Academy of Sciences. 2016;113:11525. doi: 10.1073/pnas.1613121113
64. Kim J, Kim YH, Kim J, Park DY, Bae H, Lee D-H, Kim KH, Hong SP, Jang SP, Kubota Y, et al.YAP/TAZ regulates sprouting angiogenesis and vascular barrier maturation. The Journal of Clinical Investigation. 2017;127:3441–3461. doi: 10.1172/JCI93825 [PubMed: 28805663]
65. Boopathy GTK and Hong W. Role of Hippo Pathway-YAP/TAZ signaling in angiogenesis. Frontiers in Cell and Developmental Biology. 2019;10;7:49. doi: 10.3389/fcell.2019.00049
66. Halder G and Johnson RL. Hippo signaling: growth control and beyond. Development. 2011;138:9–22. doi: 10.1242/dev.045500 [PubMed: 21138973]
67. Piccolo S, Dupont S and Cordenonsi M. The biology of YAP/TAZ: hippo signaling and beyond. Physiol Rev. 2014;94:1287–312. doi: 10.1152/physrev.00005.2014 [PubMed: 25287865]
68. Zanconato F, Cordenonsi M and Piccolo S. YAP/TAZ at the Roots of Cancer. Cancer Cell. 2016;29:783–803. doi: 10.1016/j.ccell.2016.05.005 [PubMed: 27300434]
69. Wang KC, Yeh YT, Nguyen P, Limqueco E, Lopez J, Thorossian S, Guan KL, Li YJ and Chien S. Flow-dependent YAP/TAZ activities regulate endothelial phenotypes and atherosclerosis. Proc Natl Acad Sci U S A. 2016;113:11525–11530. doi: 10.1073/pnas.1613121113 [PubMed: 27671657]
70. Giampietro C, Disanza A, Bravi L, Barrios-Rodiles M, Corada M, Frittoli E, Savorani C, Lampugnani MG, Boggetti B, Niessen C, et al.The actin-binding protein EPS8 binds VE-cadherin and modulates YAP localization and signaling. J Cell Biol. 2015;211:1177–92. doi: 10.1083/jcb.201501089 [PubMed: 26668327]
71. Sivaraj KK, Dharmalingam B, Mohanakrishnan V, Jeong HW, Kato K, Schröder S, Adams S, Koh GY and Adams RH. YAP1 and TAZ negatively control bone angiogenesis by limiting hypoxia-inducible factor signaling in endothelial cells. Elife. 2020;9:e50770 doi: 10.7554/eLife.50770
72. Byzova TV, Goldman CK, Pampori N, Thomas KA, Bett A, Shattil SJ and Plow EF. A mechanism for modulation of cellular responses to VEGF: activation of the integrins. Mol Cell. 2000;6:851–60. doi: [PubMed: 11090623]
73. Kiosses WB, Shattil SJ, Pampori N and Schwartz MA. Rac recruits high-affinity integrin alphavbeta3 to lamellipodia in endothelial cell migration. Nat Cell Biol. 2001;3:316–20. doi: 10.1038/35060120 [PubMed: 11231584]
74. Shiojima I and Walsh K. Role of Akt signaling in vascular homeostasis and angiogenesis. Circ Res. 2002;90:1243–50. doi: 10.1161/01.res.0000022200.71892.9f [PubMed: 12089061]
75. Eliceiri BP. Integrin and growth factor receptor crosstalk. Circ Res. 2001;89:1104–10. doi: 10.1161/hh2401.101084 [PubMed: 11739274]

76. Frisch SM and Screaton RA. Anoikis mechanisms. Current Opinion in Cell Biology. 2001;13:555–562. doi: 10.1016/S0955-0674(00)00251-9 [PubMed: 11544023]
77. Park M-H, Kim AK, Manandhar S, Oh S-Y, Jang G-H, Kang L, Lee D-W, Hyeon DY, Lee S-H, Lee HE, et al.CCN1 interlinks integrin and hippo pathway to autoregulate tip cell activity. eLife. 2019;8:e46012. doi: 10.7554/eLife.46012 [PubMed: 31429823]
78. Yun S, Hu R, Schwaemmle ME, Scherer AN, Zhuang Z, Koleske AJ, Pallas DC and Schwartz MA. Integrin α5β1 regulates PP2A complex assembly through PDE4D in atherosclerosis. J Clin Invest. 2019;129:4863–4874. doi: 10.1172/jci127692 [PubMed: 31408443]
79. Kim N-G and Gumbiner BM. Adhesion to fibronectin regulates Hippo signaling via the FAK–Src–PI3K pathway. The Journal of Cell Biology. 2015;210:503. doi: 10.1083/jcb.201501025 [PubMed: 26216901]
80. Astone M, Lai JKH, Dupont S, Stainier DYR, Argenton F and Vettori A. Zebrafish mutants and TEAD reporters reveal essential functions for Yap and Taz in posterior cardinal vein development. Sci Rep. 2018;8:10189. doi: 10.1038/s41598-018-27657-x [PubMed: 29976931]
81. Wang C, Zhu X, Feng W, Yu Y, Jeong K, Guo W, Lu Y and Mills GB. Verteporfin inhibits YAP function through up-regulating 14–3-3σ sequestering YAP in the cytoplasm. Am J Cancer Res. 2016;6:27–37. doi: [PubMed: 27073720]
82. Kato K, Diéguez-Hurtado R, Park DY, Hong SP, Kato-Azuma S, Adams S, Stehling M, Trappmann B, Wrana JL, Koh GY, et al.Pulmonary pericytes regulate lung morphogenesis. Nat Commun. 2018;9:2448. doi: 10.1038/s41467-018-04913-2 [PubMed: 29934496]
83. Liu-Chittenden Y, Huang B, Shim JS, Chen Q, Lee SJ, Anders RA, Liu JO and Pan D. Genetic and pharmacological disruption of the TEAD-YAP complex suppresses the oncogenic activity of YAP. Genes Dev. 2012;26:1300–5. doi: 10.1101/gad.192856.112 [PubMed: 22677547]
84. Messmer KJ and Abel SR. Verteporfin for Age-Related Macular Degeneration. Annals of Pharmacotherapy. 2001;35:1593–1598. doi: 10.1345/aph.10365

Clinical Perspective

1. **What is New?**
   - Using Cre lines that delete the HHT causing *Alk1* gene in different subsets of endothelial cells, we showed that *Alk1* deletion in capillary and venous endothelium led to arteriovenous malformations (AVMs).
   - *Alk1* mutants displayed defective polarization against the direction of blood flow in capillary and venous endothelium, as well as increased integrin-VEGFR2 mediated PI3K activation of YAP/TAZ signaling.
2. **What are the clinical implications?**
   - Pharmacological integrin inhibition using cilengitide or ATN161, or YAP/TAZ inhibition using verteporfin prevented AVM formation in *Alk1* mutant mice.
   - Our study reveals integrin and YAP/TAZ as novel effectors of ALK1 signaling and AVM pathogenesis that could be targeted for AVM treatment in HHT patients.

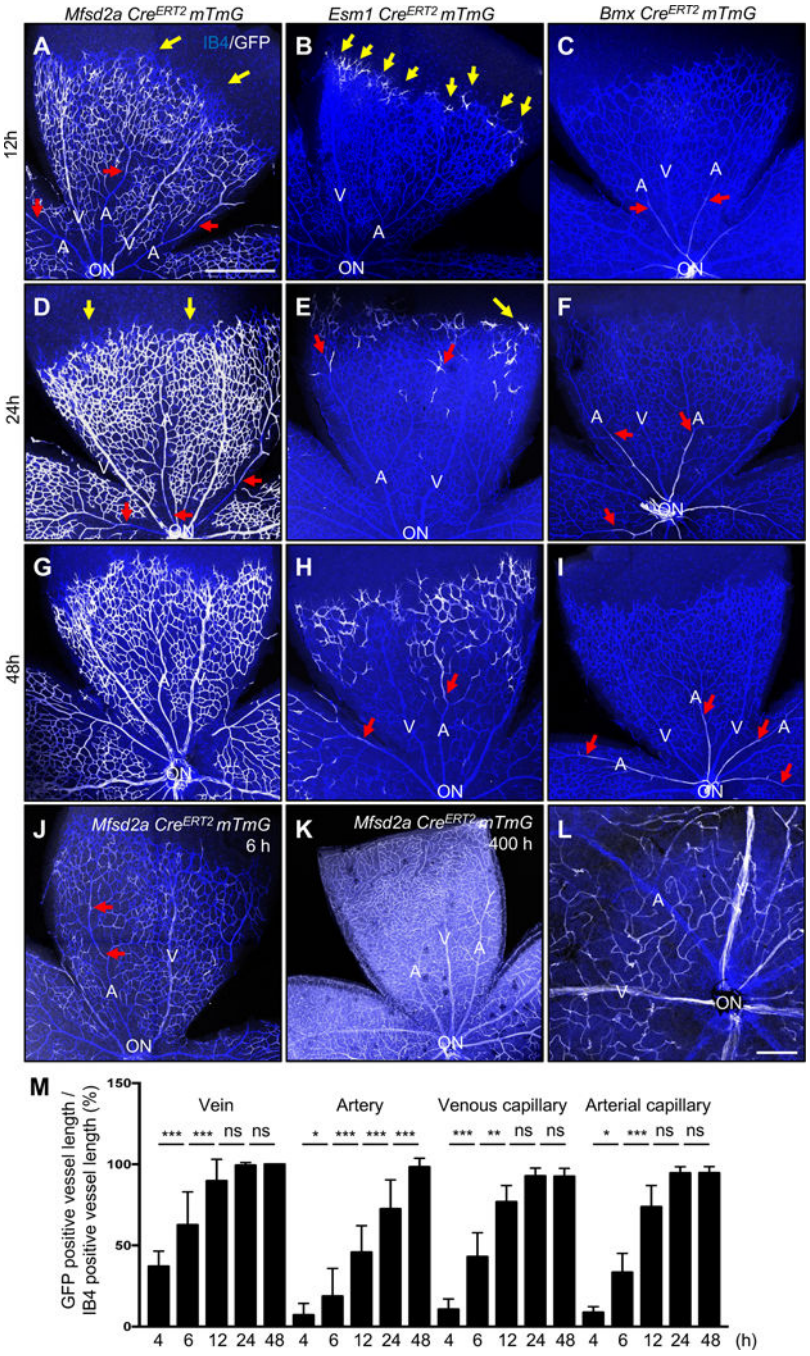

Figure 1. Retinal endothelial cell lineage tracing

(A-I) P6 retina flat mount images labeled with IB4 (blue) and GFP (white) from *Mfsd2a Cre^{ERT2} mTmG* (A, D, G), *Esm1 Cre^{ERT2} mTmG* (B, E, H) and *Bmx Cre^{ERT2} mTmG* (C, F, I) mice injected with 100 μg tamoxifen (Tx) at P5.5 (12 h, A-C), P5 (for 24 h, D-F) and P4 (for 48 h, G-I) and dissected at P6. (J) 100 μg Tx was injected at P6 and dissected after 6 h in *Mfsd2a Cre^{ERT2} mTmG* mice. (K) 100 μg Tx was injected at P4 and dissected after 400 h (P21) (L) 2 mg/kg Tx was injected in P20 *Mfsd2a Cre^{ERT2} mTmG* mice and dissect at P21. Yellow arrows indicate tip cells and red arrows indicate location of GFP-expressing ECs in

arteries. (M) Quantification of *Mfsd2a Cre^{ERT2} mTmG* GFP expressing vessel length over IB4 positive vessel length from optic nerve. n = 6–8 retinas per time point. P-value < 0.001, Error bars: SEM. *P-value < 0.05, **P-value < 0.01, ***P-value < 0.001, ns: nonsignificant, One-way ANOVA with Sidak's multiple comparisons test. ON: optic nerve, V: vein, A: artery, Scale bars: 500 μm (A-K) and 50 μm (L).

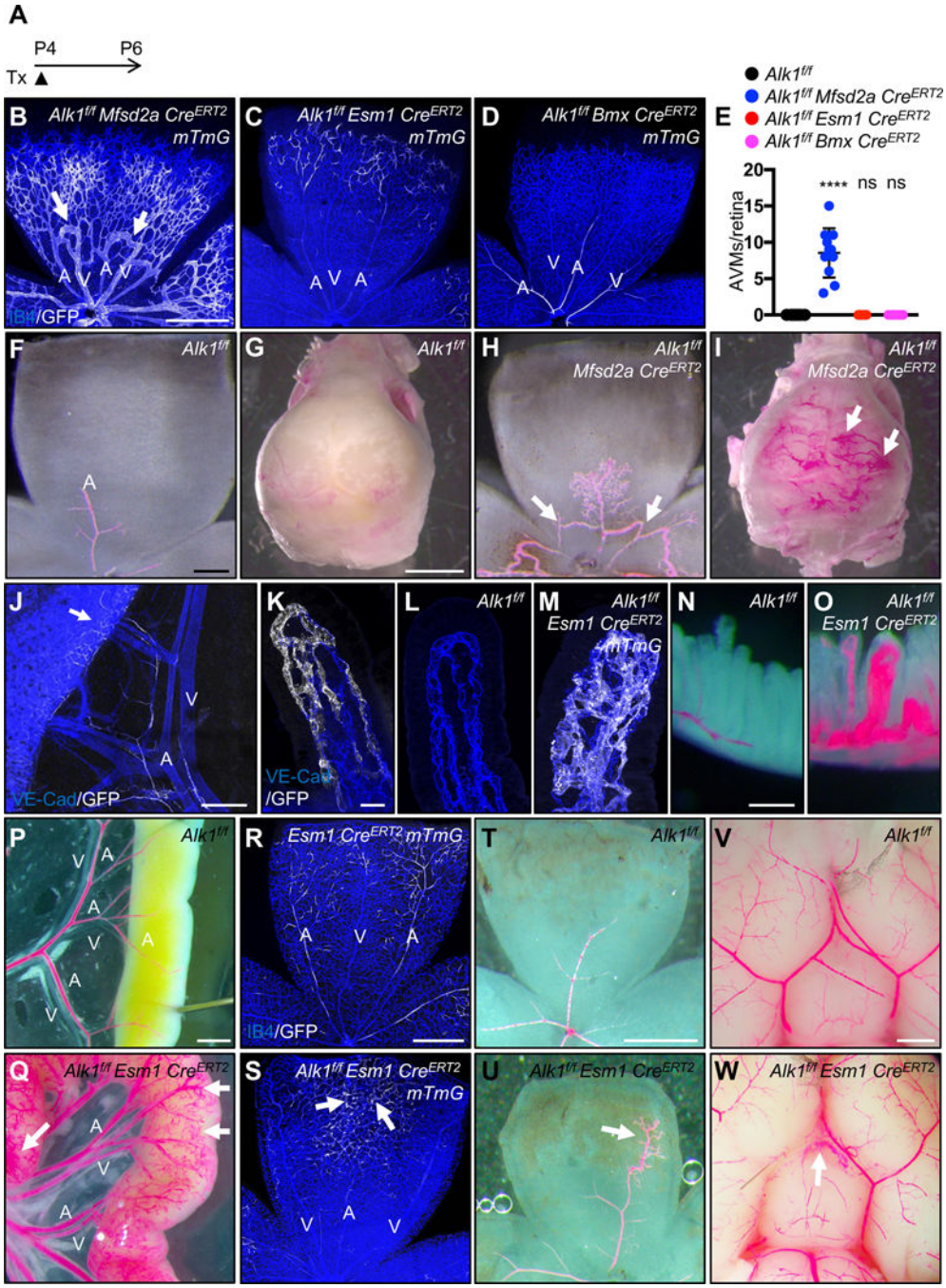

Figure 2. Capillary-venous loss of ALK1 leads to AVMs.

(A) Schematic representation of the experimental strategy used to delete *Alk1* in mice (P4-P6). (B-D) P6 retina flat mount images labeled with IB4 (blue) and GFP (white) from *Alk1*$^{f/f}$ *Mfsd2a Cre*^{ERT2} *mTmG* (B), *Alk1*$^{f/f}$ *Esm1 Cre*^{ERT2} *mTmG* (C) and *Alk1*$^{f/f}$ *Bmx Cre*^{ERT2} *mTmG* pups (D) injected with 100 μg Tx at P4 and dissected at P6. White arrows indicate AVMs. (E) Quantification of AVM number. n = 6–11 mice per group. Error bars: SEM. **** P-value < 0.0001, ns: nonsignificant, One-way ANOVA with Sidak's multiple comparisons test. (F-I) Vascular labeling with latex dye (red) of retinal and brain vessels in

Alk1$^{f/f}$ (F and G) and *Alk1*$^{f/f}$ *Mfsd2a Cre*^{ERT2} (H and I) P6 pups. White arrows indicate AVMs. (J and K) GFP (white) and VE-Cad (blue) staining of mesentery and gastrointestinal (GI) tract (J) and lacteals (K) from P14 *Esm1 Cre*^{ERT2} *mTmG*. 100 μg Tx was injected at P4. An arrow indicates *Esm1* positive capillary ECs (J). (L and M) VE-Cad (blue) and GFP (white) staining of jejunum lacteals from P14 *Alk1*$^{f/f}$ (L) and *Alk1*$^{f/f}$ *Esm1 Cre*^{ERT2} *mTmG* (M). (N-Q and T-W) 100 μg Tx was injected at P4 and dissected at P12. Vascular labeling with latex dye (red) of villi, GI tracts, retinas and brains in *Alk1*$^{f/f}$ (N,P,T and V) and *Alk1*$^{f/f}$ *Esm1 Cre*^{ERT2} (O, Q, U and W) P12 pups. (R and S) 100 μg Tx was injected at P4 and dissected at P12 (R and S). IB4 (blue) and GFP (white) staining of retinal flat mounts from *Esm1 Cre*^{ERT2} *mTmG* (R) *and Alk1*$^{f/f}$ *Esm1 Cre*^{ERT2} *mTmG* (S) P12 mice. An arrow indicates vascular malformations (Q, U and W). A: artery, V: vein, Scale bars: 500 μm (B-D), 200 μm (F and H), 2 mm (G and I). 400 μm (J), 25 μm (K-M), 200 μm (N and O), 1 mm (P-G and V-W), 500 μm (R-U), 200 μm.

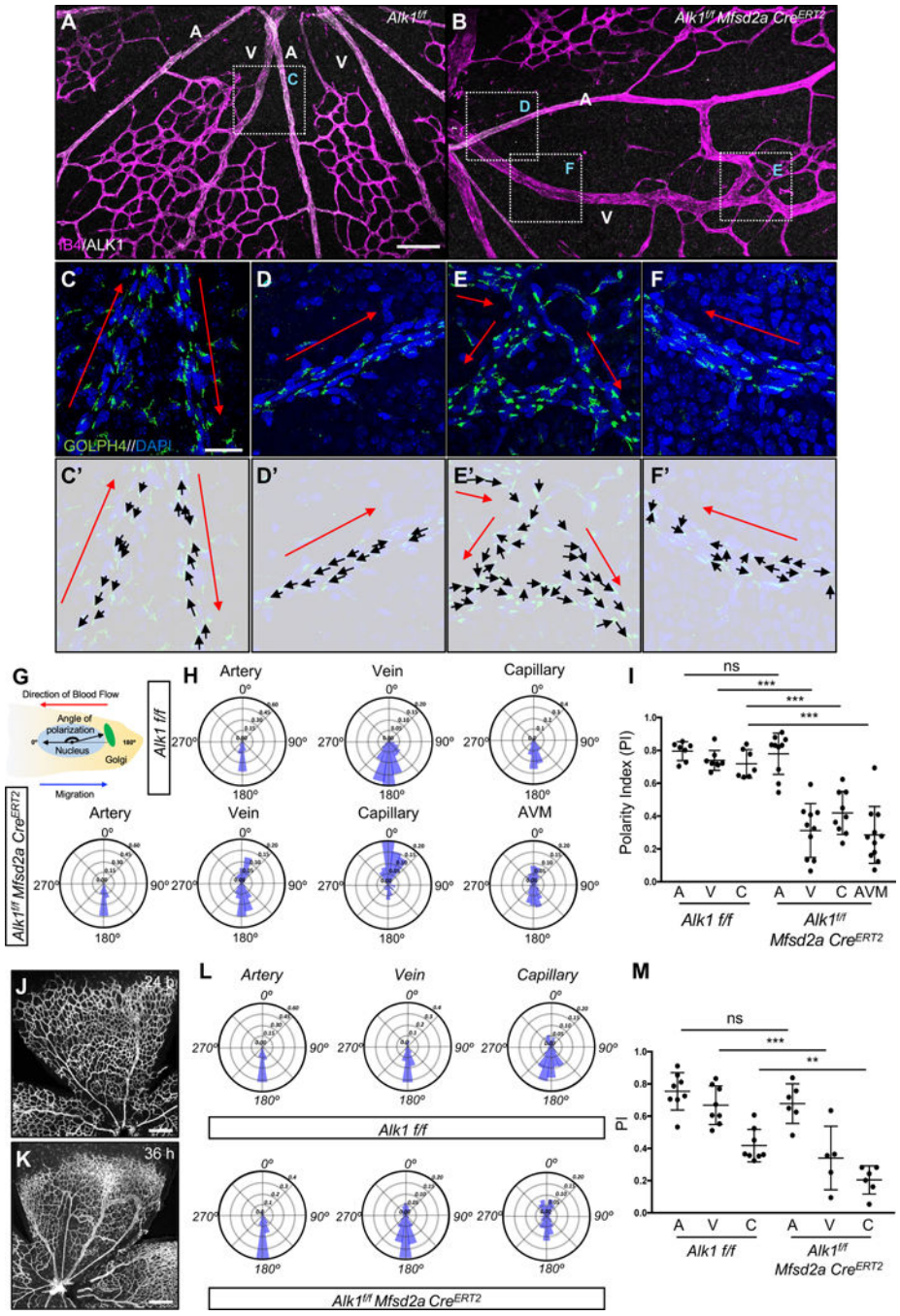

Figure 3. ALK1 controls cell polarization against the blood flow direction.

(A-B) IB4 (Magenta) and ALK1 (white) staining of retinal flat mounts from *Alk1*$^{f/f}$ (A) and *Alk1*$^{f/f}$ *Mfsd2a Cre*^{ERT2} (B) pups injected with 100 μg Tx at P4 and dissected at P6. (C-F) Higher magnification of insets in A and B. GOLPH4 (green) and DAPI (blue) staining of retina flat mounts. Red arrows indicate the blood flow direction. (C'-F') Background images from Figure 2C–2F and corresponding polarity vectors (black arrows). (G) The polarity axis of each cell was defined as the angle between the direction of blood flow and the cell polarity axis, defined by a vector drawn from the center of the cell nucleus to the center

of the Golgi apparatus. (H) Angular histograms showing the distribution of polarization angles of ECs in the artery, vein and capillaries from *Alk1*$^{f/f}$ and artery, vein, capillary and AVM from *Alk1*$^{f/f}$ *Mfsd2a Cre*^{ERT2} mouse retinas. n = 7–11 retinas. (I) polarity index (PI) box plots of ECs from artery, vein and capillary from *Alk1*$^{f/f}$ and artery, vein, capillary and AVM from *Alk1*$^{f/f}$ *Mfsd2a Cre*^{ERT2} P6 retinas. n = 7–11 retinas. (J and K) IB4 (gray) staining of retinal flat mounts from *Alk1*$^{f/f}$ *Mfsd2a Cre*^{ERT2} pups injected with 100 μg at P4 and dissected after 24 h (P5) (J) and 36 h (P5.5) (K). (L) Angular histograms showing the distribution of polarization angles of ECs in the artery, vein and capillary from *Alk1*$^{f/f}$ and *Alk1*$^{f/f}$ *Mfsd2a Cre*^{ERT2} P5 retinas at 24 h after Tx injection. (M) PI box plots of ECs from artery, vein and capillary from *Alk1*$^{f/f}$ and *Alk1*$^{f/f}$ *Mfsd2a Cre*^{ERT2} retinas at 24 h after Tx injection. n = 5–8 retinas/group. Error bars: SEM. **P-value < 0.01, ***P-value < 0.001, ns: nonsignificant, Two-way ANOVA with Tukey's multiple comparisons test. Scale bars: 100 μm (A-B), 20 μm (C-F) and 500 μm (J-K)

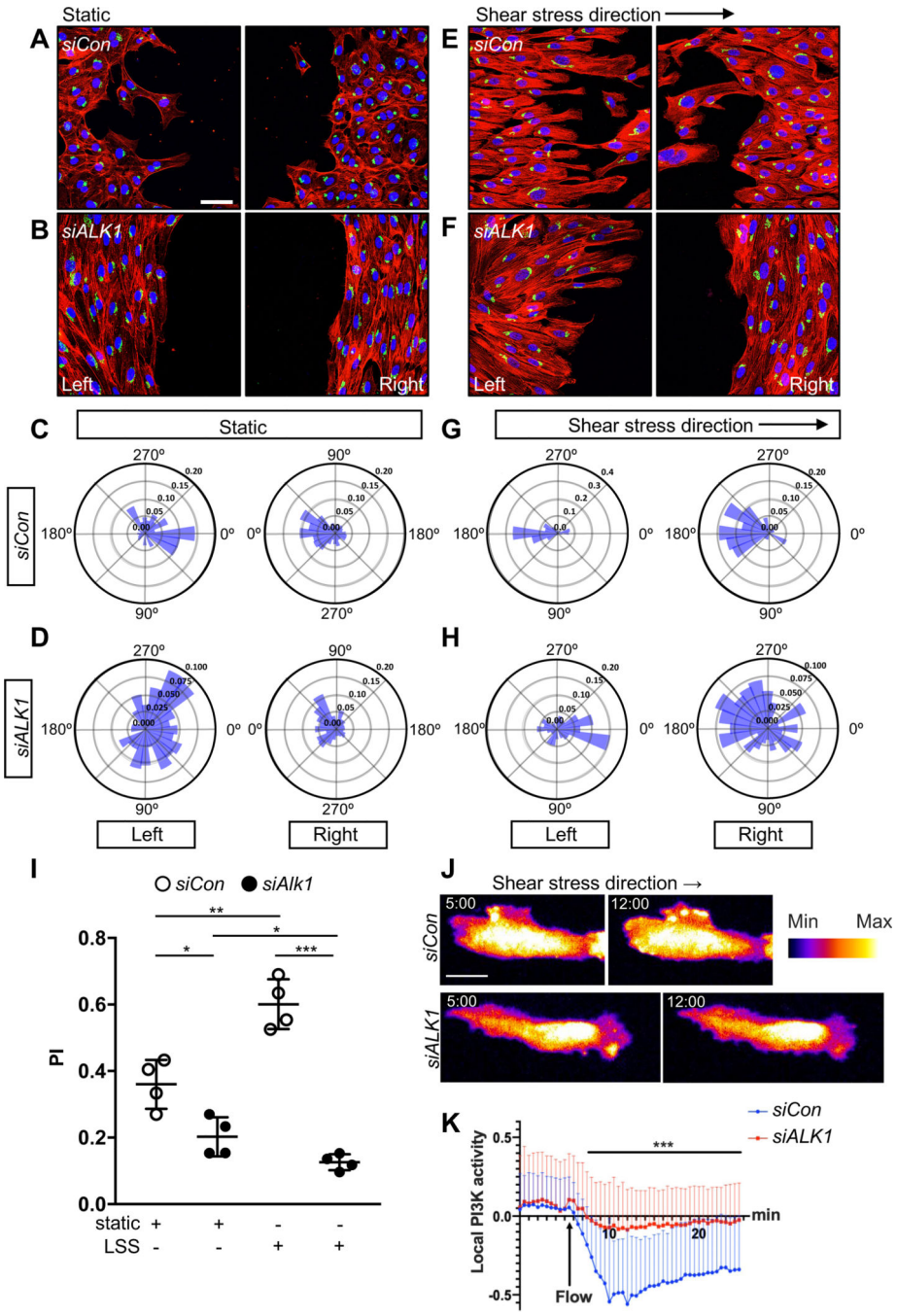

Figure 4. ALK1 controls EC polarization against the flow direction *in vitro*.

(A-B) Representative images of scratch wound assays after 18 h showing polarity angles of HUVECs transfected with Control (*siCon*) (A) or *ALK1* (*siALK1*) (B) siRNAs under static conditions and immunolabeled with phalloidin(red), GM130 (green), and DAPI (blue). (E-F) Representative images of scratch wound assays showing polarity angles of *siCon* (E) or *siALK1* (F) HUVECs with 18 h exposure to laminar shear stress (LSS) at 15 dynes/cm^2. Left panels are upstream and right panels are downstream of flow. (C-D and G-H) Angular histograms showing polarization angles of *siCon* (C and G) or *siALK1* ECs (D and

H) at 18 h after scratch with (G-H) or without (C-D) LSS. Left is upstream and right is downstream of flow (G and H). (I) PI box plots of upstream (left) scratch areas from *siCon* or *siALK1* transfected HUVECs at 18 h after with or without LSS. (C-I) n=6–8 images from 3 independent experiments. Error bars: SEM. *P-value < 0.05, **P-value < 0.01, ***P-value < 0.001, Two-way ANOVA with Sidak's multiple comparison test. (J) Representative time lapse images of *siCon* or *siALK1* HUVECs stably transduced with PH-AKT-mClover3 and plasma membrane targeting sequence of LCK-mRuby3. HUVEC monolayers in microfluidic chambers were exposed to 12 dynes/cm^2 LSS under the microscope. 5 min (static) and 12 min (LSS) images were selected from the movies. The surface is color-coded by the value of PH-AKT intensity. (K) Local activation of PI3K was quantified by image analysis. PH-AKT intensity was normalized with average static intensity at each time point. 0 – 5 min : static and 5 – 24.5 min : LSS, n= 61, 41 cells from 3 independent experiments, Error bar : SEM. ***P-value < 0.001, Two-tailed unpaired t-test between *siCon* and *siALK1* in average over the time. Scale bars : 50 μm (A-B and E-F), 20 μm (J).

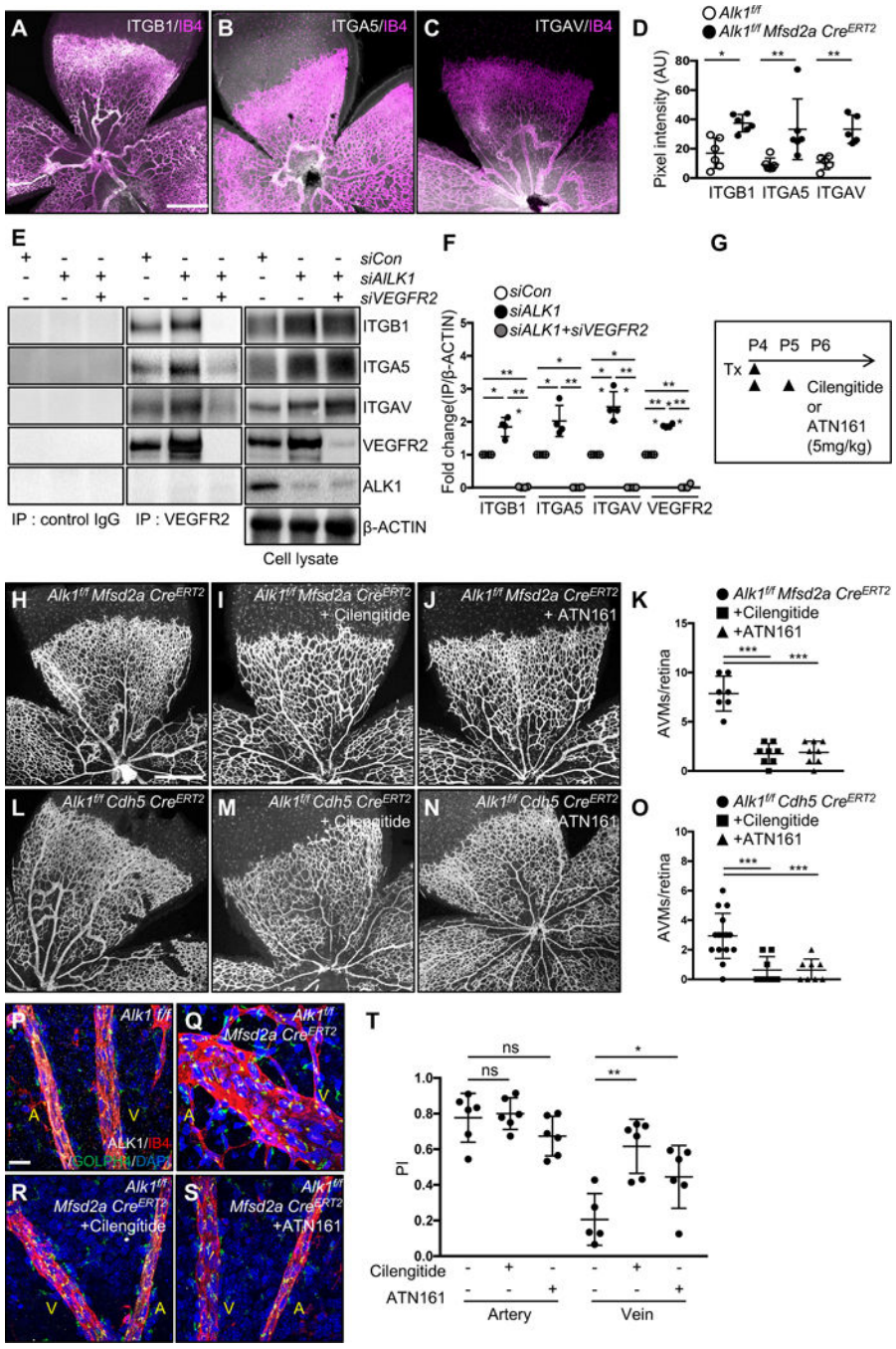

Figure 5. Integrin inhibition prevents AVM formation in *Alk1* mutant retinas.

(A-C) IB4 (Magenta) and ITGB1(A, white), ITGA5 (B, white) or ITGAV (C, white) staining of retinal flat mounts from P8 *Alk1*$^{f/f}$ *Mfsd2a Cre*^{ERT2} pups. (D) Quantification of ITGB1, ITGA5 and ITGAV in P8 *Alk1*$^{f/f}$ *Mfsd2a Cre*^{ERT2} retinas. (E) VEGFR2 immunoprecipitation in *siCon*, *siALK1* or *siALK1+siVEGFR2* HUVECs and western blot analysis for ITGB1, ITGA5, ITGAV and ALK1. VEGFR2, ITGB1, ITGA5, ITGAV, ALK1 and β-ACTIN expression from the total cell lysates are shown as loading controls. Rabbit IgG was used as control. (F) Quantification of ITGB1, ITGA5 or ITGAV levels from

immunoprecipitation normalized to β-ACTIN from total cell lysates. *P<0.05, **P<0.01, ***P-value < 0.001, One-way ANOVA with Sidak's multiple comparisons test. (G) Experimental strategy to assess the effects of integrin inhibitors in *Alk1* deleted retinas. Arrowheads indicate the time course of Tx (100 μg) and cilengitide (5mg/kg), ATN161 (5mg/kg) or vehicle administration. (H-J and L-N) IB4 staining of P6 retinal flat mounts from *Alk1*$^{f/f}$ *Mfsd2a Cre*^{ERT2} (H-J) or *Alk1*$^{f/f}$ *CDH5 Cre*^{ERT2} (L-N) injected with cilengitide (I and M) or ATN161 (J and N) at P4 and P5. (K and O) Quantification of the AVM number. Each dot represents one retina. n = 7–16 retinas per group. Error bars: SEM. ***P-value < 0.001, One-way ANOVA with Sidak's multiple comparisons test. (P-S) IB4 (Magenta), ALK1 (white), GOLPH4 (green) and DAPI (blue) staining of retina flat mounts from *Alk1*$^{f/f}$ (P), *Alk1*$^{f/f}$ *Mfsd2a Cre*^{ERT2} (Q), Cilengitide (R) or ATN161 (S) injected *Alk1*$^{f/f}$ *Mfsd2a Cre*^{ERT2} pups. A: artery, V: vein, (T) PI box plots of ECs from artery and vein from *Alk1*$^{f/f}$ *Mfsd2a Cre*^{ERT2} injected cilengitide or ATN161 retinas. n=5–8 retinas/group. Error bars: SEM. *P-value < 0.05, **P-value < 0.01, ns: nonsignificant, One-way ANOVA with Sidak's multiple comparisons test. Scale bars: 500 μm (A-C, G-I and K-M), 20 μm (P-S).

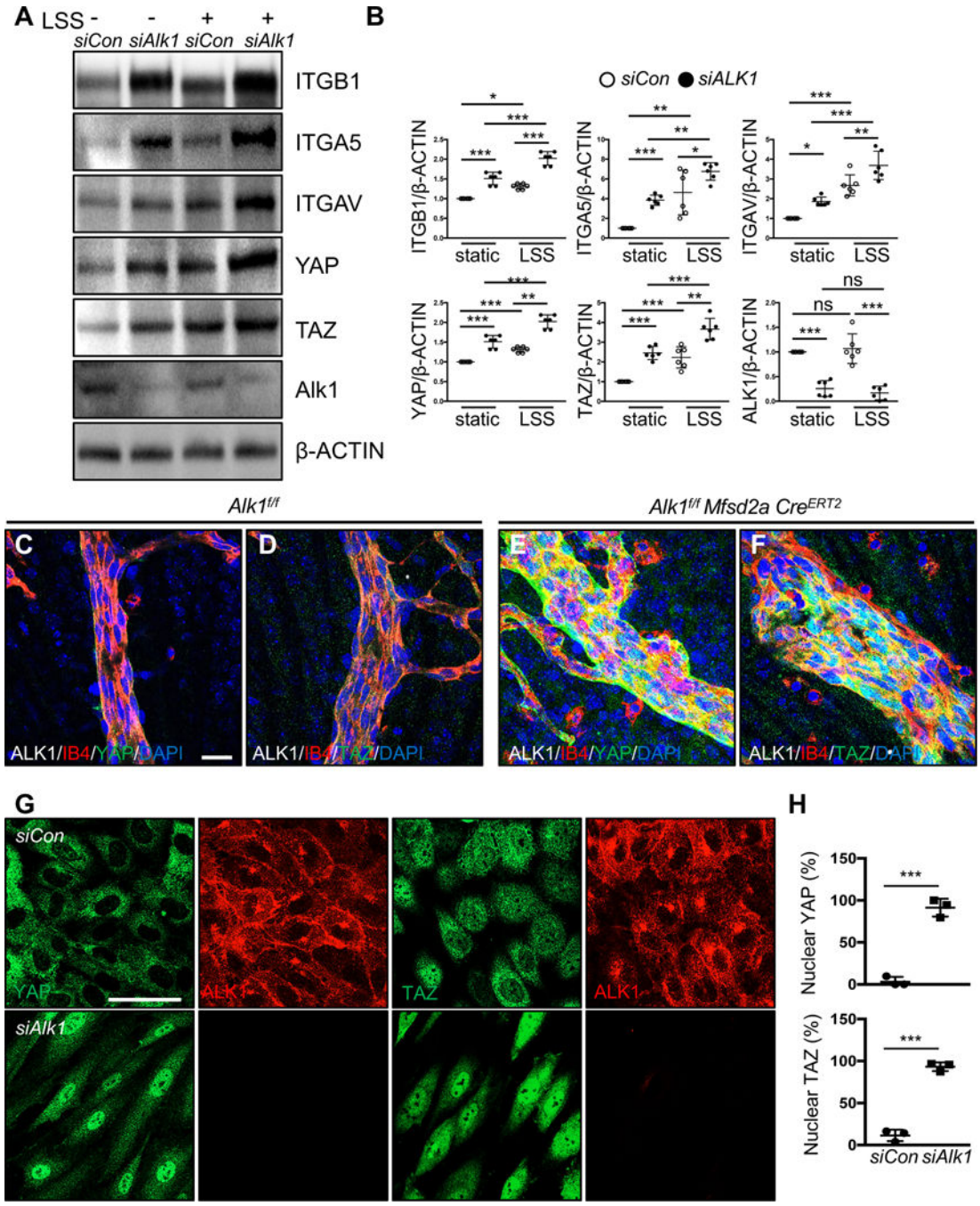

Figure 6. ALK1 controls YAP/TAZ expression and localization.

(A) Western blot analysis of HUVECs transfected with control and *ALK1* siRNAs followed by 18 h exposure to LSS (15 dynes/cm^2). (B) Quantification of ITGB1, ITGA5, ITGAV, YAP or TAZ levels normalized to β-ACTIN. *P<0.05, **P<0.01, ***P<0.001, Two-way ANOVA with Sidak's multiple comparison test. (C-F) YAP and TAZ (green), ALK1 (gray), IB4 (red), DAPI (blue) staining of retinal flat mounts from P8 *Alk1$^{f/f}$* (C-D) or *Alk1$^{f/f}$ Mfsd2aCre^{ERT2}* (E-F) pups. A scale bar: 20 μm (C-F) (G) YAP or TAZ (green) and ALK1 (red) staining of *siCon* and *siALK1* HUVECs. A scale bar: 50 μm. (H) Quantification of

nuclear YAP and TAZ from *siCon* and *siALK1* transfected HUVECs. ***P<0.001, n = 3 independent experiments. Two-tailed unpaired t-test between *siCon* and *siALK1*.

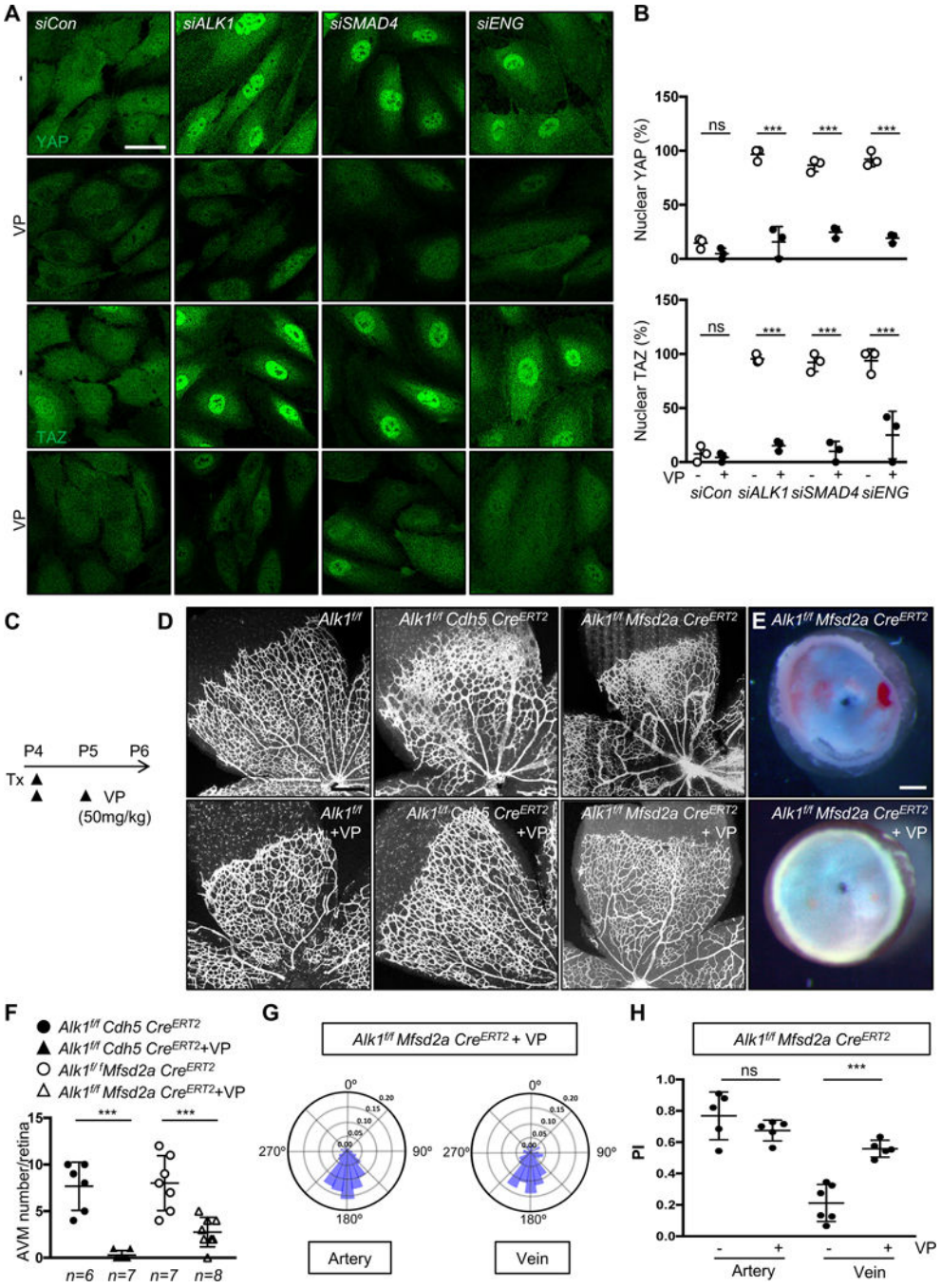

Figure 7. YAP/TAZ inhibition improves AVM formation in *Alk1* mutant retinas.

(A) YAP and TAZ staining of *siCon*, *ALK1*, *SMAD4* or *ENG* siRNAs transfected HUVECs treated with DMSO or Verteporfin (VP, 5 μM) for 6 h. Nuclear YAP/TAZ localization in *siALK1*, *siSMAD4* or *siENG* ECs is blocked by VP treatment. A scale bar: 50 μm. (B) Quantification of nuclear YAP and TAZ from *siCon*, *siALK1,siSMAD4 and siENG* transfected HUVECs. ***P<0.001, ns: nonsignificant, Two-way ANOVA with Tukey's multiple comparisons test. (C) Experimental strategy to assess the effects of YAP/TAZ inhibition in EC specific *Alk1* deleted vasculature. Arrowheads indicate the time course of

Tx (100 μg) and VP (50mg/kg) or vehicle administration. (D) IB4 staining of P6 retinal flat mounts from VP injected *Alk1*$^{f/f}$, *Alk1*$^{f/f}$ *CDH5 Cre*^{ERT2} or *Alk1*$^{f/f}$ *Mfsd2a Cre*^{ERT2} mice. (E) Stereomicroscopy images of vehicle or VP injected *Alk1*$^{f/f}$ *Mfsd2a Cre*^{ERT2} retinas. (F) Quantification of the AVM number/retina. Each dot represents one retina. n = 6–8 retinas per group. Error bars: SEM. ***P-value < 0.001, One-way ANOVA with Sidak's multiple comparisons test. (G) Angular histograms showing polarization angles of artery and vein from *Alk1*$^{f/f}$ *Mfsd2a Cre*^{ERT2} with VP. (H) PI box plots of *Alk1*$^{f/f}$ *Mfsd2a Cre*^{ERT2} with vehicle or VP. n=5–6 retinas, Error bars: SEM, ***P-value < 0.001, ns: nonsignificant, Two-way ANOVA with Tukey's multiple comparisons test. Scale bars : 50 μm (A), 500 μm (D), 300 μm (E)

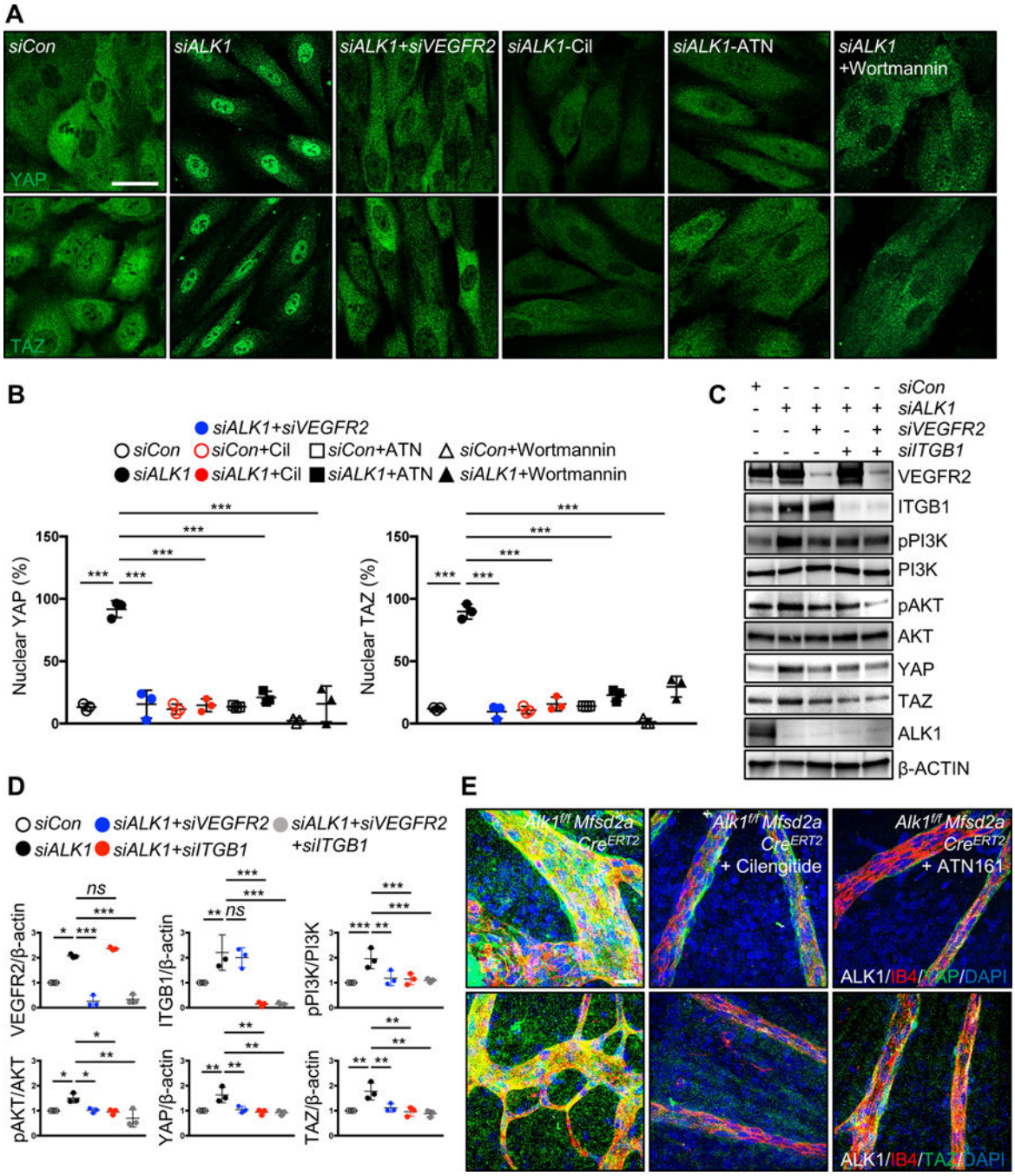

Figure 8. VEGFR2, integrin and PI3K function upstream of YAP/TAZ in Alk1 mutants

(A) YAP and TAZ staining for *siCon*, *siALK1* and *siALK1+siVEGFR2* transfected HUVECs and *ALK1* siRNA transfected HUVECs treated with cilengitide (Cil, 5 μM), ATN161 (ATN, 5 μM) and wortmannin (100 mM) for 12 h. Nuclear YAP/TAZ localization in *siALK1* ECs is blocked by *siVEGFR2,* cilengitide, ATN161 and wortmannin treatment. (B) Quantification of nuclear YAP and TAZ from for *siCon*, *siALK1* and *siALK1+siVEGFR2* transfected HUVECs and *ALK1* siRNA transfected HUVECs treated with cilengitide, ATN16, wortmannin. ***P<0.001, n = 3 independent experiments. Error

bars: SEM. ***P-value < 0.001, Two-way ANOVA with Tukey's multiple comparisons test. (C) Western blot analysis of HUVECs transfected with control, *ALK1, ALK1+VEGFR2, ALK1+ITGB1* or *ALK1+VEGFR2+ITGB1* siRNAs. (D) Quantification of pPI3K/PI3K, pAKT/AKT and YAP or TAZ levels normalized to β-ACTIN. *P<0.05, **P<0.01, ***P<0.001, ns: nonsignificant, One-way ANOVA with Sidak's multiple comparisons test. (E) YAP and TAZ (green), ALK1 (white), IB4 (red) and DAPI (blue) staining of retinal flat mounts from cilengitide or ATN161 injected $Alk1^{f/f}$ *Mfsd2a* Cre^{ERT2} P6 mice. Scale bars: 50 μm (A), 20 μm (E)